



Available online at www.sciencedirect.com



PALAEO

Palaeogeography, Palaeoclimatology, Palaeoecology 235 (2006) 265–287

www.elsevier.com/locate/palaeo

Simulations of ecosystem response during the sapropel S1 deposition event

D. Bianchi ^{a,*}, M. Zavatarelli ^a, N. Pinardi ^a, R. Capozzi ^a, L. Capotondi ^b,
C. Corselli ^c, S. Masina ^d

^a Università di Bologna, Centro Interdipartimentale per la Ricerca sulle Scienze Ambientali, Via S. Alberto 163, 48100 Ravenna, Italy

^b ISMAR, Istituto di Scienze del Mare, C.N.R., Via Gobetti 101, 40129 Bologna, Italy

^c Università di Milano-Bicocca Dipartimento di Scienze Geologiche e Geotecnologiche, Piazza dell'Ateneo Nuovo 1, 20126 Milan, Italy

^d Istituto Nazionale di Geofisica e Vulcanologia, Via Donato Creti 12, 40128 Bologna, Italy

Accepted 12 September 2005

Abstract

A one-dimensional ecosystem numerical model is used to simulate the ecosystem changes that could have occurred in the open ocean areas of the Eastern Mediterranean Sea during the Climatic Optimum interval (9500–6000 B.P., Mercone et al. [Mercone, D., Thomson, J., Croudace, I.W., Siani, G., Paterne, M., Troelstra, S., 2000. Duration of S1, the most recent sapropel in the eastern Mediterranean Sea, as indicated by accelerator mass spectrometry radiocarbon and geochemical evidence. *Paleoceanography* 15, 336–347]). In this period the S1 sapropel was deposited. S1 is the most recent sapropel in the succession of organic carbon-rich layers intercalated in normal Neogene sedimentary sequences. Different theories have been invoked in order to explain the deposition of this peculiar layer. Our simulations seem to indicate that the modified thermohaline circulation, supplying oxygen only in the first 500 m of the water column, is responsible for the sapropel deposition when higher productivity is allowed in the euphotic zone. The model shows the importance in this process of bacteria that consume oxygen by decomposing the Particulate Organic Matter (POM) produced in the upper water column. The sinking velocity of POM partially regulates the timescale of the occurrence of anoxia at the bottom and in the whole water column, allowing the relatively rapid onset of sapropel deposition.

© 2005 Elsevier B.V. All rights reserved.

Keywords: Sapropel; Holocene; Marine ecology; Mediterranean Sea; Ecological modelling

1. Introduction

1.1. Background

The eastern Mediterranean is a concentration basin with a thermohaline circulation of anti-estuarine type, maintained by the excess of evaporative losses over the precipitation and river runoff inputs (Fig. 1). The fresh-

water deficit is compensated by the surface inflow through the Sicily Channel of the so-called Modified Atlantic Water (MAW), constituting the surface branch of the anti-estuarine thermohaline circulation cell. The returning branch is located at intermediate depths and is formed by a well-defined water mass, the Levantine Intermediate Water (LIW), formed in limited areas of the eastern Mediterranean in winter. The LIW flow crosses the Sicily Channel and spreads into the western Mediterranean at a depth range of 300–500 m, exiting the Mediterranean Sea through the Gibraltar Straits.

* Corresponding author. Fax: +39 0544937323.

E-mail address: d.bianchi@sincem.unibo.it (D. Bianchi).



Fig. 1. Schematic of the Mediterranean Sea thermohaline circulation. The grey lines indicate the surface/intermediate water mass circulation forced by Gibraltar Atlantic inflow and Levantine Intermediate Water (LIW) formation processes occurring in the northern Levantine basin. The black lines indicate the meridional vertical circulation in western and eastern Mediterranean forced by the deep water formation processes occurring in the Gulf of Lions and in the Southern Adriatic. Redrawn from Pinardi et al. (2005), reprinted with permission.

The source of the Eastern Mediterranean Deep Water (EMDW) is located in the Adriatic Sea, but a dramatic change in the site of the EMDW formation was recently observed by Roether et al. (1996). The spreading of the EMDW from its formation area provides the basic ventilation mechanism for the deep eastern Mediterranean basin.

The anti-estuarine circulation and low river runoff promote strong oligotrophic conditions in open waters, revealed by mean primary production rates among the lowest observed (Bethoux, 1989). The low surface productivity affects the sedimentary features of the basin: recent sediments from open sea regions in the eastern Mediterranean are typically characterized by an average total organic carbon concentration of around 0.3%, and higher concentrations are thought to be indicative of different environmental conditions (Murat and Got, 2000). However, the paleoceanographic record suggests that the Mediterranean circulation, ecosystem and deep sedimentary processes have not always been the same as they are today.

Neogene sedimentary sequences of the eastern Mediterranean Sea are characterized by the periodic occurrence of dark, organic-rich layers, the so-called sapropels (Olausson, 1961; Cita et al., 1977; Vergnaud-Grazzini et al., 1977; Rossignol Strick et al., 1983; Kroon et al., 1998; Emeis et al., 2000 among others) that according to the definition of Kidd et al. (1978) show >2% in organic matter content.

The sapropel sequences show a cyclicity correlated to the insolation changes due to orbital parameters, in particular there is a close correspondence between sapropel deposition and minima of the precession index (Rossignol-Strick, 1983; Hilgen, 1991). It was

hypothesized that during precession minima the increased seasonal thermal gradient between ocean and continental regions enhanced the monsoonal circulation system. The strengthened African and Indian monsoon could promote a larger Nile river discharge (Rossignol-Strick, 1985) and the potential “greening of the Sahara”, i.e., the (re)activation of the currently fossil river system of the North African margin (Rohling et al., 2002; Larrasoña et al., 2003). Moreover, the precipitation in the northern borderlands of the eastern Mediterranean increased, providing therefore an additional freshwater input to the basin (Rohling, 1994). Much evidence suggests that this kind of climatic pattern characterized the most recent sapropel S1 (Krom et al., 1999; Martínez-Ruiz et al., 2000) deposited between 9.5 and 6 ky B.P. (Mercone et al., 2000).

The S1 deposition event extended for a period of 2500–3500 years. A 200-year interruption was found in Adriatic and Aegean sediment cores. This interruption corresponds to a cooler period that occurred between 7100 and 6900 years B.P. (Rohling et al., 1997; De Rijk et al., 1999), where less organic matter was found in the sediments.

1.2. Hypothesis on sapropel deposition

Several models have been proposed to explain the sapropel deposition. However, two hypotheses have received the greatest attention: decreased ventilation of deep layers that caused anoxia of the deep water column promoting the preservation of the organic carbon in the newly deposited sediments, otherwise subject to bacterial remineralization (*stagnation model*) and enhancement of the surface primary production,

determining a consequent increase in organic matter fluxes to the bottom where organic material is buried and preserved in the sediments (*increased productivity model*).

According to the stagnation model, an increased freshwater input would establish a low-salinity surface layer, thus modifying the thermohaline circulation of the eastern Mediterranean by weakening/preventing the EMDW formation and then promoting the non-ventilation of the deep waters. Lacking an efficient ventilation mechanism, the deep waters were gradually depleted of oxygen until the establishment of truly anoxic conditions. Under such conditions the aerobic bacterial organic matter remineralization is inhibited, and the accumulation and preservation of organic carbon in the sediments is made possible (Hartnett et al., 1998; Cramp and O'Sullivan, 1999). This hypothesis appears to be supported by several biogeochemical features identified in some sapropels: the absence of benthic fauna (Jorissen, 1999), the lack of bioturbation and the preservation of the original lamination in well-preserved sapropels (Kemp et al., 1999), the enrichment in trace-metal content (Warning and Brumsack, 2000), and the isotopic composition of Fe-sulfide species (Passier et al., 1999a). Additionally, the presence in some sapropels of biomarkers produced by photosynthetic anaerobic bacteria suggests the presence of anoxic conditions in the lower part of the euphotic zone (Bosch et al., 1998; Passier et al., 1999b) which in the eastern Mediterranean can be as deep as 150 m.

The increased productivity model in its original formulation (Calvert, 1983; Pedersen and Calvert, 1990) postulates a significant enhancement of primary productivity and organic matter fall out, without invoking drastic changes in the thermohaline circulation and in the aerobic remineralization processes. This hypothesis is supported by the composition of nannofossil assemblages in eastern Mediterranean sapropels (Castadori, 1993), and the analysis of the Barium profile within the sapropels (Van Santvoort et al., 1997).

Recently many authors have suggested the likely concurrence of both stagnation and increased productivity during sapropel deposition due to the modified climatic and oceanographic conditions of the eastern Mediterranean (e.g. Rohling and Gieskes, 1989; Howell and Thunnell, 1992; Rohling, 1994; Strohle and Krom, 1997).

The orbitally driven shift toward humid conditions and the increase in river runoff during sapropel times provides a supporting setting for both the stagnation and increased productivity hypothesis. The enhanced river runoff supplies an immediate nutrient input

(Wehausen and Brumsack, 1999; Martinez-Ruiz et al., 2000, 2003), promotes a stable stratification of the water column and eventually the shallowing of the nutricline within the euphotic zone supporting the development of a highly productive Deep Chlorophyll Maximum (DCM) (Rohling, 1994; Sachs and Repeta, 1999). At the same time the formation of a less saline surface layer preventing dense-water formation could provoke the halting of oxygen ventilation in the deep layers.

The work by Myers et al. (1998) added further evidence supporting the stagnation hypothesis by simulating the Mediterranean Sea thermohaline circulation during the Holocene by means of a Mediterranean Sea general circulation model capable of reproducing the present-day and Holocene circulations. They used different reconstructions of the sea surface paleotemperatures and paleosalinities based on oceanographic proxies (Kallel et al., 1997). Their simulations showed a weakening of the anti-estuarine circulation cell in the eastern Mediterranean, the shallowing of the winter convection depth up to 200–450 m and the isolation and stagnation of the deeper water masses. Stratford et al. (2000) coupled the same model to a simple nutrient-cycling biogeochemical model based on phosphate, organic detritus and dissolved oxygen. Their results indicate that with a threefold increase (with respect to present) of nutrient riverine input, anoxic conditions develop at 450–500 m depth in about 1000 years. The anoxic area expands toward the bottom with a velocity of 500 m every 100 years. Under such an enhanced nutrient input the open sea regions of the eastern Mediterranean exhibit an organic carbon flux at the seafloor of $3.3\text{--}6.6 \text{ mg C m}^{-2} \text{ day}^{-1}$. This model does not however explicitly resolve the processes of oxygen consumption due to bacteria, owing to the model's simplicity.

The dynamics of the anoxic conditions in the eastern Mediterranean during the Holocene were deduced by Strohle and Krom (1997) by dating the onset of sapropel S1 layers sampled at different depths. The authors hypothesize the formation of a minimum in the oxygen concentration at the basis of the LIW layer and the subsequent formation and expansion toward the seafloor of an anoxic zone (with a deepening velocity analogous to the one observed in the simulations of Stratford et al., 2000).

Despite the remarkable amount of information acquired on the possible dynamics of the sapropel event, many questions remain open. There are uncertainties on the extent of the increase in primary production, on the causes that induced this increase and on its localization

in the water column. As previously stated, the enhanced river runoff supported an increased input of nutrients. Nevertheless, some authors (Sachs and Repeta, 1999) suggest that this additional input would not be enough to sustain the production increase observed during sapropel deposition. Alternative models to the river-driven nutrient supply have as common denominator the hypothesis of productivity concentrated in a DCM supported by strong stratification in the euphotic zone. Strong stability of the surface layers, and the shoaling of the nutricline within the euphotic zone, would favour the growth of specialized phytoplanktonic communities adapted to a deep nutrient source (Sachs and Repeta, 1999). It is suggested that mat-forming diatoms could have provided the largest contribution to the organic carbon flux to the seafloor during sapropel deposition (Pearce et al., 1998; Kemp et al., 1999).

Another controversial point concerns the presence and extent of anoxic/dysoxic conditions during sapropel times and their role in organic carbon preservation. Even if the presence of anoxic/dysoxic conditions in the sediments appears undisputed there are still uncertainties about their vertical extension in the water column: some authors set limits to their presence to a layer (anoxic ‘blanket’, Casford et al., 2003) directly above the sediment/water interface, other suggest that they could have concerned a wide stagnating water mass located below a well-oxygenated mixed layer (Strohle and Krom, 1997; Murat and Got, 2000; Stratford et al., 2000). Thus the evolution of the anoxic zone in the water column is not clear; if it developed in the upper water column to reach subsequently the seafloor or originated at the bottom remains an open question. The timing and duration of the process are also not completely clear.

In this work we investigate, by means of a one-dimensional ecosystem model implemented in the eastern Mediterranean, the possible concurrent role of the stagnation and the enhanced productivity hypothesis in establishing the deposition of the S1 sapropel, trying to gain more insight on the dynamics of the development of anoxic conditions in the water column.

2. The numerical model

2.1. The coupled modelling system

The ecosystem model used is the one-dimensional modular ecosystem model, MEM-1D, originating by the coupling of the one-dimensional version of the Princeton Ocean Model (Blumberg and Mellor, 1987) with the European Regional Ecosystem Model,

ERSEM (Baretta et al., 1995). Such a model has already been used to simulate present-day conditions in several parts of the Mediterranean Sea (Allen et al., 1998, 2002; Vichi et al., 2003).

The Princeton Ocean Model has been used here in “diagnostic” mode: the time-dependent vertical profiles of temperature and salinity were imposed from the simulation of Myers et al. (1998), while the model only computes the vertical profiles of vertical diffusion coefficients through the Mellor and Yamada (1982) second order turbulence closure model. The coefficients are used to compute the vertical profiles of the biogeochemical state variables. Other physical processes not explicitly resolved by the one-dimensional model, such as large scale upwelling/downwelling and lateral ventilation are parameterized as detailed in the appendix.

ERSEM is a generic biomass-based ecosystem model constituted of a set of differential equations describing the fluxes of carbon macronutrients (nitrogen, phosphorous and silica) and oxygen between the different compartments of the marine ecosystem. A schematic representation of the trophic interactions between different groups is shown in Fig. 2. The biological components are aggregated in functional groups belonging to specific trophic levels with distinctive ecological functions. Each functional group represents a set of species linked by similar ecological behaviour rather than close phylogenetic affinity. The definition of a functional group has an implicit allometric connotation, since the functionalities of an organism are usually correlated to its dimension. The modelling of the functional groups follows the idea of a “standard organism” described by physiological activities such as ingestion, assimilation, respiration, excretion, and egestion, and population processes such as growth and mortality. Each standard organism is expressed in terms of internal carbon, nitrogen, phosphorous and silicon concentrations, without invoking fixed ratios among such elements, but dynamically determining the functional ratios between the chemical components. Appendices A.1 and A.2 provide a synthetic description of the main equations of the physical and biogeochemical models.

The pelagic submodel prognostically calculates the water column concentrations of dissolved nutrients (phosphate, nitrate, ammonia and silicate), oxygen, phytoplankton, zooplankton, bacteria and particulate organic matter (POM). The phytoplankton pool is divided into three functional groups, diatoms, picophytoplankton, and phytoflagellates. Diatoms are the only group requiring silica as an internal nutrient. Moreover, they differ from the other phytoplanktonic functional

groups by being subject to sinking. The sinking velocity is a function of the nutrient limitation conditions and can achieve a maximum value of 5 m day^{-1} under maximal nutrient limitation. Primary production is forced by the incident solar radiation scaled by a factor that determines the Photosynthetically Available Radiation (PAR) and by nutrient concentration. Nutrient uptake is controlled by the difference between the external nutrient concentrations and the time dependent internal C/N/P ratios. The zooplankton functional groups are mesozooplankton, microzooplankton and heterotrophic flagellates; only a functional group for pelagic aerobic bacteria is considered. Mesozooplankton, characterized by fixed C/N/P ratios, feed on diatoms, flagellates and microzooplankton. Microzooplankton, heterotrophic flagellates and pelagic bacteria, each characterized by varying C/N/P ratios form the microbial loop: heterotrophic flagellates graze bacteria and picophytoplankton, and are consumed by microzooplankton; microzooplankton feed on diatoms, flagellates and are grazed by mesozooplankton; pelagic bacteria feed on the dissolved and particulate organic carbon produced by all living groups by exudation and excretion and on particulate detritus. Detritus remineralization by the bacterial component is the main oxygen sink in the aphotic water column while oxygen sources are physical aeration at the surface and primary production related inputs. Details on bacterial dynamics and oxygen consumption are

provided in Appendix A.3. Biogenic detritus sedimentation velocity is fixed at 1.5 m day^{-1} , and represents the main coupling between pelagic and benthic submodels, providing the forcing for the benthic submodel.

The benthic submodel prognostically calculates the concentration of aerobic and anaerobic bacteria, pore water nutrient concentration, benthic gases and different reactive forms of organic detritus. The only feedback between pelagic and benthic submodels, besides detritus sedimentation, is represented by diffusion of nutrients and oxygen between pore water and the upper water column.

For a detailed description of ERSEM version used in this work see Varela et al. (1995) for the primary production processes, Baretta-Bekker et al. (1995) for the microbial loop dynamics, Broekhuizen et al. (1995) for mesozooplankton dynamics, Ebenhoh et al. (1995) and Ruardij and Van Raaphorst (1995) for the benthic submodel.

2.2. Model implementation and setup

The one-dimensional model has been implemented in the area of the Urания, Discovery, Atalante and Bannock anoxic basins in the Ionian Sea (Fig. 3), a region with a mean depth of 3046 m. The water column is discretized by 40 levels with a logarithmic distribution in the first 140 m and a constant distribution below. The model time step is 1728 s.

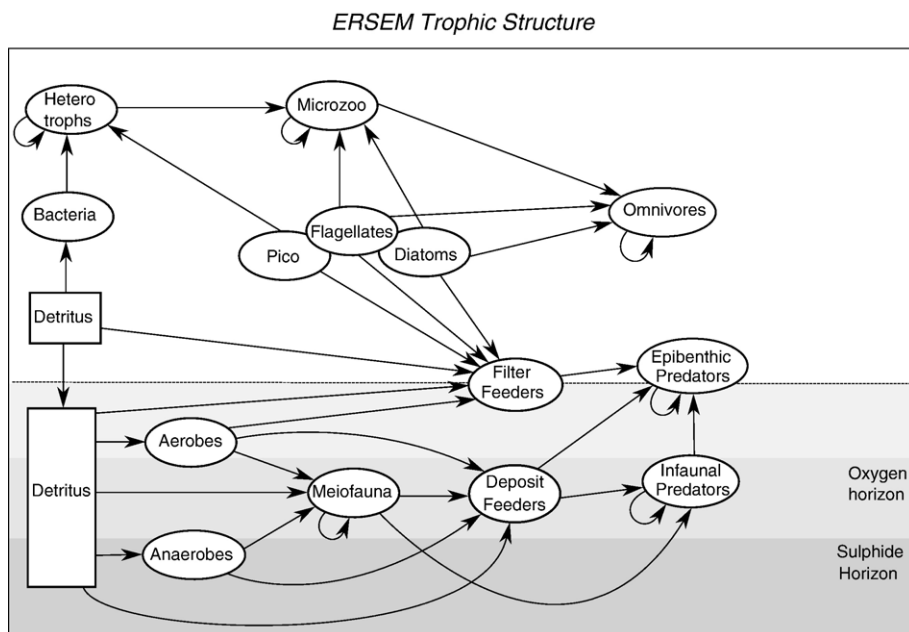


Fig. 2. A schematic diagram of ERSEM ecosystem structure. From Allen et al. (1998), reprinted with permission.

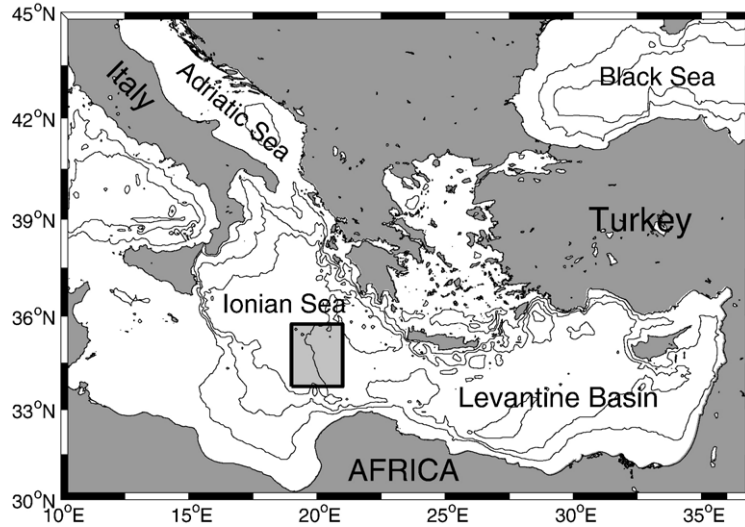


Fig. 3. Area of implementation of the model.

Temperature and salinity data used for the numerical experiments are taken from the present-day and the main Holocene experiments of the Mediterranean Sea general circulation by Myers et al. (1998). We recall here that such simulations were carried out by imposing at the model surface present-day Sea Surface Temperature (SST) and Salinity (SSS) fields for the present-day experiment and present-day SST and SSS reconstruction by Kallel et al. (1997) for the Holocene experiment. The annual SST and SSS cycles in the area of implementation of the one-dimensional model for both simulations are shown in Fig. 4A and B respectively. The SST (Fig. 4A) is the same for the two scenarios and shows a marked seasonal cycle; the maximum values are reached in August and the lowest between February and March. The Climatic Optimum SSS (Fig. 4B) is about 2 psu lower with respect to the present-day field. Wind stress forcing for the present-day simulations is obtained by the European Centre for Medium-Range Weather Forecast (ECMWF) fields, while paleowinds for the Holocene are taken from the simulations of Dong and Valdes (1995). Monthly mean values for wind stress were averaged over the implementation area and applied to the model by a linear time interpolation. The annual wind stress modulus cycles for both the simulations considered are shown in Fig. 4C. It can be noted that wind stress is stronger during the Holocene, in particular during winter and summer; maximum values are reached between May and June for the present day and between December and March for the Holocene.

Monthly temperature and salinity profiles from the simulations of Myers et al. (1998) averaged over the

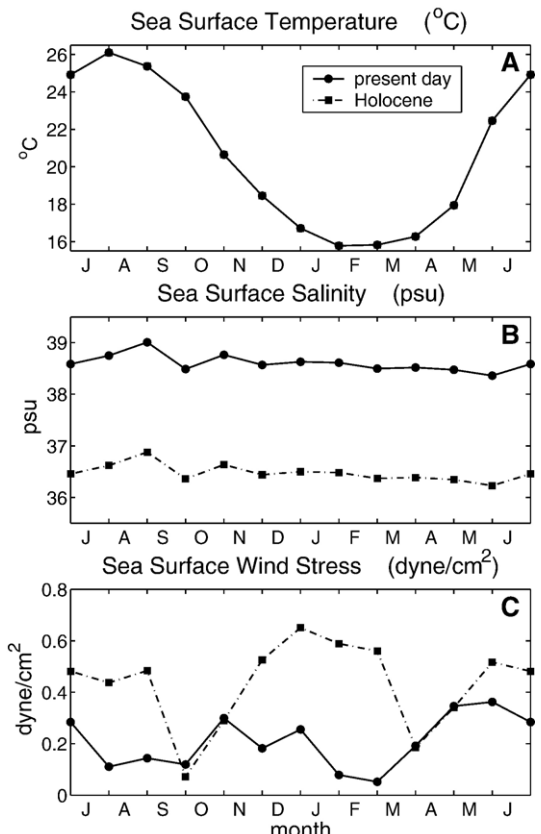


Fig. 4. Sea surface temperature (A), sea surface salinity (B) and wind stress (C) for the present-day and Holocene physical conditions over the area of implementation of the one-dimensional model. Units are °C for temperature, psu for salinity and dyn cm^{-2} for wind stress.

area indicated in Fig. 3 were extracted from the simulation results and diagnostically imposed with a linear time interpolation between adjacent monthly mean values. The resulting annual cycle of temperature salinity and σ_t profiles for both the present day and the Holocene are shown in Fig. 5. The seasonal temperature cycle (Fig. 5A, B) is essentially identical in both cases, while the salinity profiles (Fig. 5C, D) reflect the freshening imposed by the use of low

paleosalinity values. In term of density profiles (Fig. 5D, E) the summer stratification period is more extended in time in the Climatic Optimum case with respect to the present-day case. It should be noted that even though the Holocene winds are stronger, stratification is similar between the Holocene and present-day conditions. This might be due to the effect of enhanced gravitational stability against mixing of the water column.

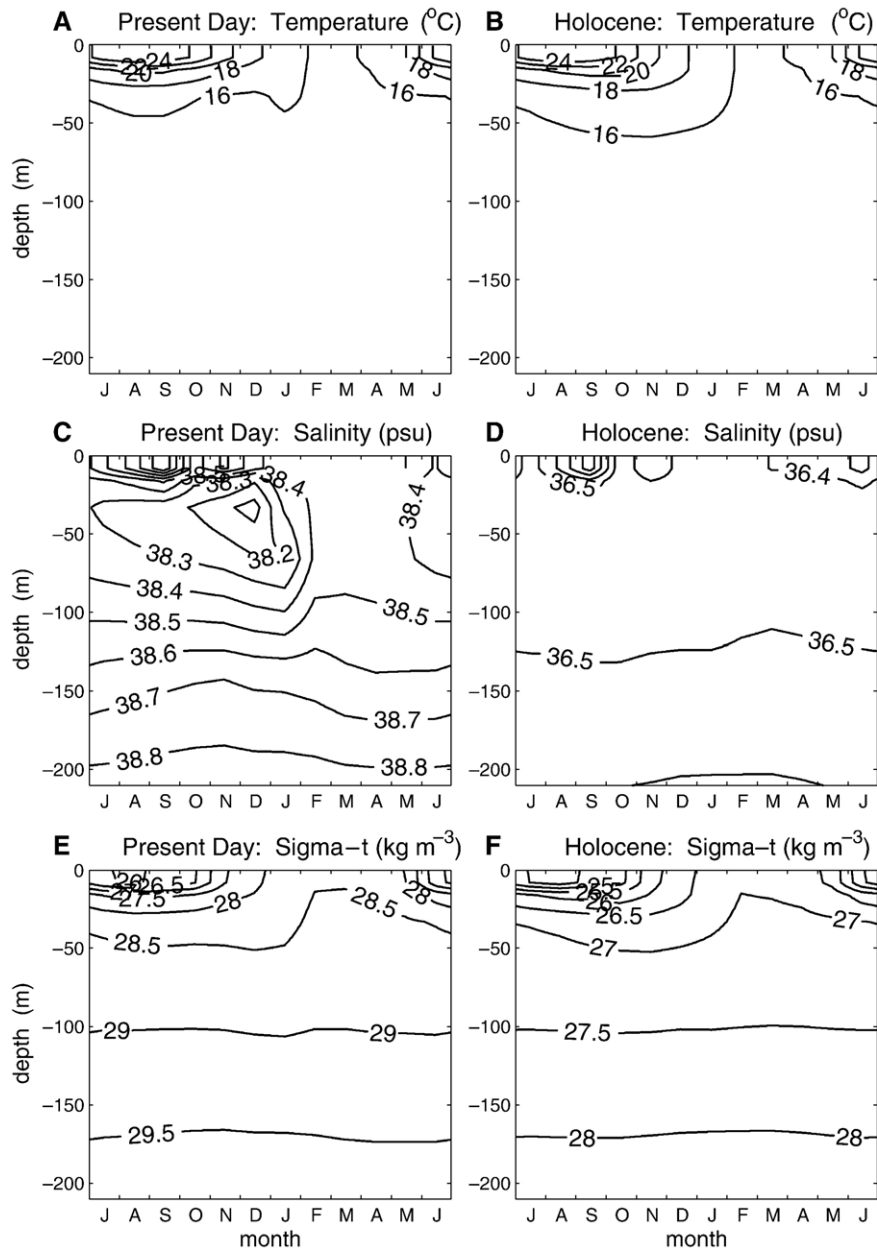


Fig. 5. Temperature, salinity and σ_t profiles for the present-day (A, C, E) and Holocene (B, D, F) physical conditions. Units are $^{\circ}\text{C}$ for temperature, psu for salinity and kg m^{-3} for σ_t .

In order to take into account the large scale Ekman pumping induced by wind stress curl in the Ionian basin (Pinardi and Navarra, 1993), a small upwelling velocity is introduced in the physical component of the one-dimensional model as detailed in Appendix A.4.

The diagnostic implementation of the one-dimensional model physical component does not require any use of heat flux as surface boundary condition for temperature. However, information on the surface solar radiation flux is required for the biogeochemical model, since this is the fundamental forcing for the primary production processes. This forcing has been implemented into the model by computing daily values for clear sky conditions. The amount of solar radiation reaching the sea surface is proportional to the length of the day but uniform during the day. The effect of clouds on the solar radiation flux at the sea surface was not taken into account due to the total lack of information on the cloud cover conditions during the Climatic Optimum. How-

ever, we performed sensitivity experiments (not shown) for the present-day simulations by using a solar radiation monthly climatology that accounts for cloud cover, from COADS data (Da Silva et al., 1995). The use of this more realistic forcing for the ecosystem resulted in a reduced primary productivity, but this reduction (9% at most) did not alter the ecosystem evolution with clear sky solar radiation.

As for the biogeochemical model, nutrient (Phosphate, Nitrate, Silicate) and oxygen initial conditions were obtained from the measurements carried out by Bregant et al. (1990) in the Bannock basin (Fig. 6). The initialization of the phytoplankton functional groups was estimated from the Ionian Sea chlorophyll-a measurements (occurring in summer) of Rabitti et al. (1994). Other biological functional groups (zooplankton, pelagic and benthic bacteria) were initialized as constant vertical profiles on the basis of the very scarce and scattered informations relative to the Ionian Sea.

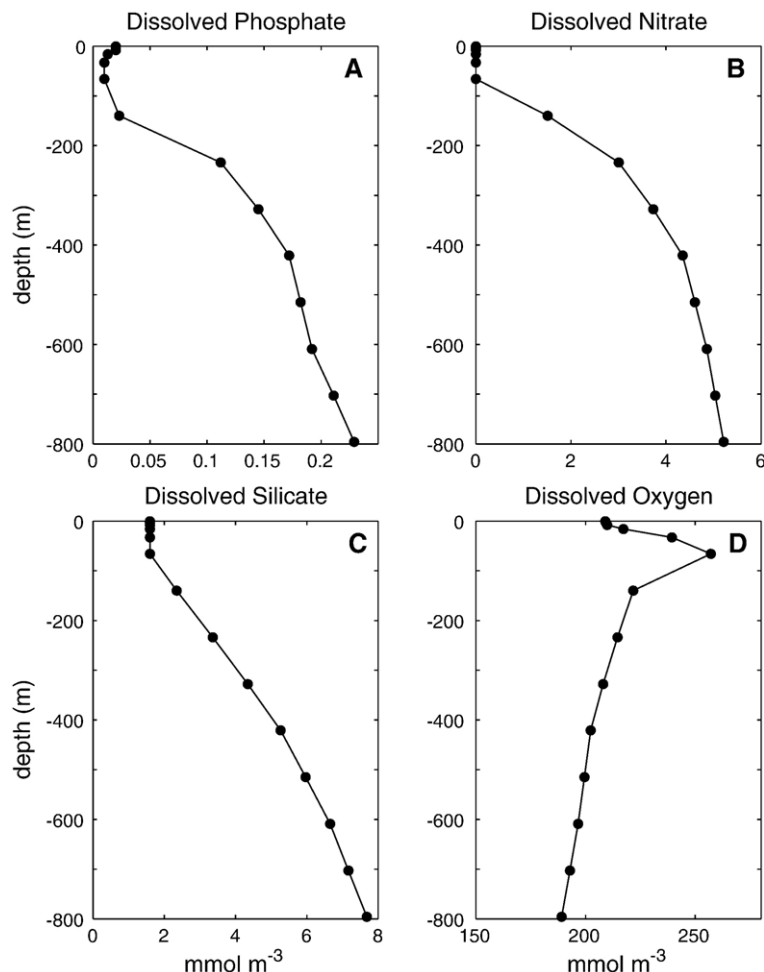


Fig. 6. Initial profiles of dissolved phosphate, nitrate, silicate and oxygen. Units are mmol m^{-3} .

Table 1
Surface nutrient concentrations (mmol m^{-3}) for the different model configurations

	Surface concentration (mmol m^{-3})		
	Phosphate	Nitrate	Silicate
Present-day	No prescribed concentration at the surface		
Reconstruction 1	0.03	0.48	0.45
Reconstruction 2	0.04	0.64	0.6

For the present-day simulation no surface nutrient concentration was applied to the model. For the paleo-simulations we choose to parameterize the supposed enhanced nutrient concentrations thought to be one of the triggers for the sapropel deposition, by imposing higher (with respect to present) surface nutrient concentrations using the formulation given in Appendix A.2. The three sets of surface nutrient concentration values used for the simulations are listed in Table 1. The Reconstruction 1 and Reconstruction 2 nutrient concentration sets are consistent with the present day observed surface nutrient concentrations in the Middle Adriatic Sea (Zavatarelli et al., 1998) and assume that the nutrient relative proportions are in Redfield balance (Redfield et al., 1963).

As suggested by the results of Myers et al. (1998) one of the most significant differences between present-day and Holocene circulation was the different depth of penetration of the EMDW. The inhibition of the deep winter mixing in the Holocene simulation and the consequent missing ventilation of the deep water masses can have a crucial effect on the oxygen supply to the deep layers in the eastern Mediterranean. In order to take in account the role of horizontal advection lateral ventilation (in a one-dimensional modelling framework) we parameterized the lateral water column ventilation process with the procedure described in Appendix A.5. According to the water mass circulation simulated by Myers et al. (1998) the lateral ventilation is introduced from the surface to the bottom for the present-day simulation and from the surface to the depth of 500 m for the Holocene simulation (see Table 2).

In the first part of the work six experiments were performed to assess the impact of both physical conditions and nutrient input on deep water sedimentation and oxygen content. The list of the simulations is given in Table 2. Three experiments (*Now Low*, *Now 1* and *Now 2*) were performed under present-day physical conditions using different prescribed (and progressively increasing) surface nutrient concentrations; the three remaining experiments (*Holo Low*, *Holo 1* and *Holo 2*) were performed under physical

conditions for the Holocene using the three nutrient reconstructions.

The *Now Low* experiment is thus performed with present-day physical conditions, wind stress forcing, lateral ventilation and no prescription of the surface nutrient concentration/nutrient input and can be considered a control simulation indicative of the present-day ecosystem dynamics in the open Ionian Sea. The *Holo Low* Experiment uses the Holocene physical conditions but the present-day surface nutrient conditions. Experiments *Holo 1* and *Holo 2* are paleosimulations with physical conditions, wind stress forcing and lateral oxygen ventilation down only to 500 m appropriate for the Holocene Climatic Optimum. The prescribed surface nutrient concentrations are indicative of higher values with respect to present.

In order to be consistent with the initial conditions all the simulations were started from the month of July. The integration time for all the simulations is 2000 years, thought to be appropriate to reproduce significant processes from a paleoceanographic point of view.

3. Model results

3.1. Ecosystem and productivities

The seasonal profiles of chlorophyll-a and the seasonal cycle of the euphotic zone vertically integrated net primary productivity for the six experiments are shown in Figs. 7 and 8 respectively; Table 3 reports the annual mean integrated primary productivities and annual mean organic carbon sedimentation fluxes at the depth of 500 m (the lower limit of water mass reventilation for the Holocene circulation) and at the bottom. All the results are averaged over the last 100 years of simulation. Annual mean primary productivities show a significant range of variations induced by the increased surface nutrient concentration, changing from the *Now Low* and *Holo Low* oligotrophic values ($125 \text{ mg C m}^{-2} \text{ day}^{-1}$) to the much higher values arising from experiments *Holo 2* and *Now 2* ($1995\text{--}2420 \text{ mg C m}^{-2} \text{ day}^{-1}$).

Table 2
Summary of the main experiments

		Experiment	Physical conditions	Reventilation depth	Surface nutrients
Now Low	Present-day		0–3000 m		Present-day
Now 1	Present-day		0–3000 m		Reconstruction 1
Now 2	Present-day		0–3000 m		Reconstruction 2
Holo Low	Holocene		0–500 m		Present-day
Holo 1	Holocene		0–500 m		Reconstruction 1
Holo 2	Holocene		0–500 m		Reconstruction 2

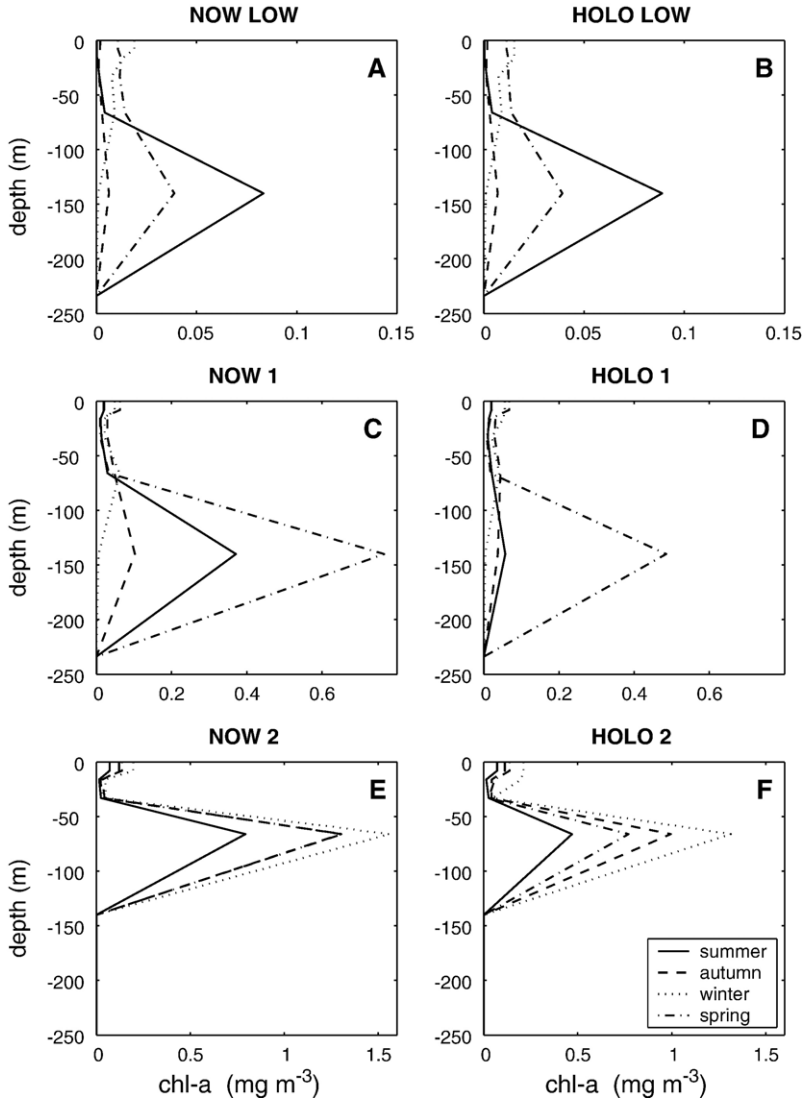


Fig. 7. Seasonal chlorophyll-a profiles for the NOW and HOLO experiments. Units are mg m^{-3} .

The experiments *Now Low* and *Holo Low* do not show marked differences in terms of ecosystem structure and both reproduce features typical of present-day oligotrophic regions. Productivity reaches maximum values during summer (Fig. 8A, B) and drops to very low values during autumn and winter. In both experiments chlorophyll-a (Fig. 7A, B) shows a well-defined summer deep maximum (DCM) localized around 140 m depth, with concentrations of about $0.1 \text{ mg chl-a m}^{-3}$. The DCM is a typical feature of present-day open Mediterranean waters; in the eastern Basin DCMs are observed at depths between 70 and 130 m (Ediger and Yilmaz, 1996; Moutin and Rainbault, 2002; Casotti et al., 2003); deeper DCMs are observed in open-sea regions of the central and

southern Ionian and Levantine Basins. The dominant phytoplankton group in the DCM is picophytoplankton. Autotrophic flagellates are found at depths shallower than 70 m and show a peak between surface and 40 m in late winter and a less intense subsurface (40–70 m) spring bloom. Diatoms are essentially absent in both simulations. Zooplankton biomasses are very low, being not sustained by the phytoplankton biomass. The dominance of picophytoplanktonic groups over larger primary producers is a significant feature observed in oligotrophic waters, both in oceanic (Li et al., 1983) and Mediterranean ecosystems (Magazzù and Decembrini, 1995), in particular in the eastern Mediterranean (Ignatiades et al., 2002; Casotti et al., 2003) characterized by more oligotrophic con-

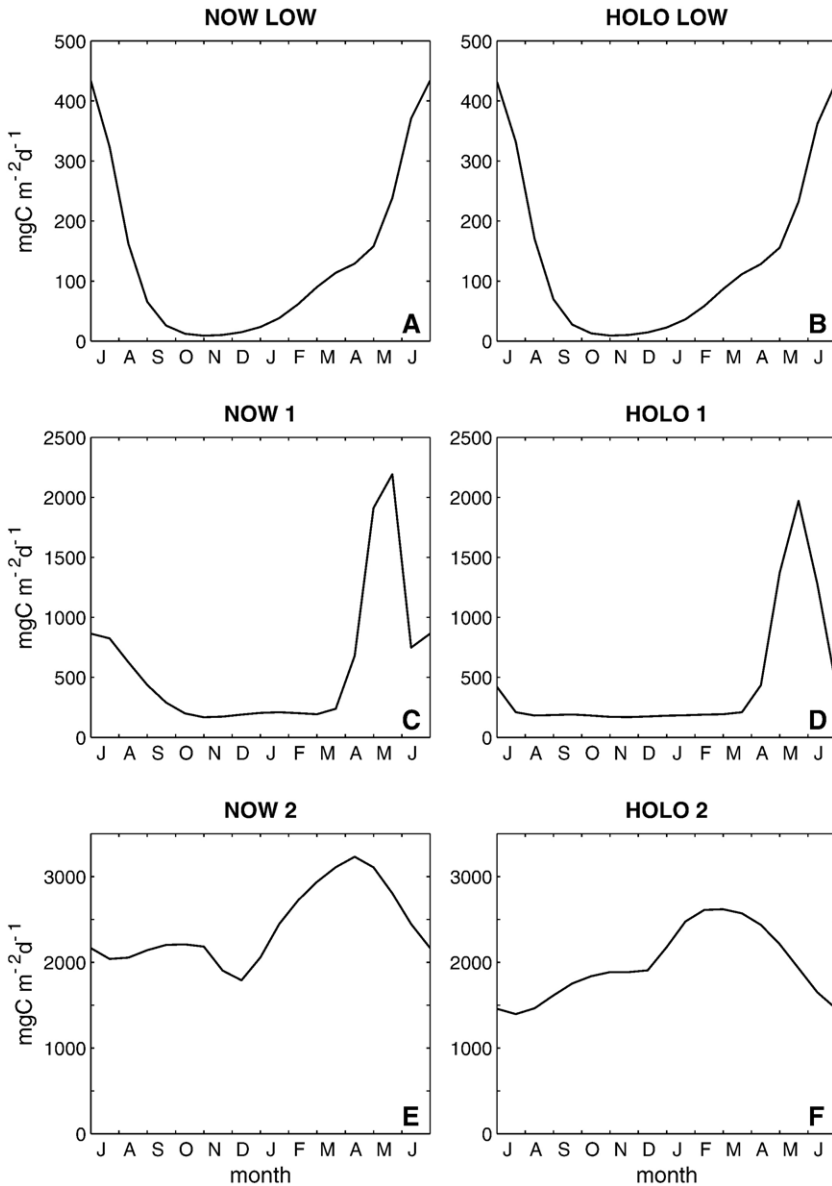


Fig. 8. Vertically integrated net primary productivity for the NOW and HOLO experiments. Units are $\text{mg C m}^{-2} \text{ day}^{-1}$.

ditions than the western Mediterranean (Bethoux, 1989).

The annual mean value of primary productivity ($125 \text{ mg C m}^{-2} \text{ day}^{-1}$ for both simulations, see Table 3) is in good agreement with the range of $114.0\text{--}268.8 \text{ mg C m}^{-2} \text{ day}^{-1}$ reported by Magazzù and Decembrini (1995) and the observations for the spring period ($208\text{--}324.5 \text{ mg C m}^{-2} \text{ day}^{-1}$, Casotti et al., 2003) and the early summer period ($159\text{--}325 \text{ mg C m}^{-2} \text{ day}^{-1}$, Moutin and Rainbault, 2002) in the Ionian Sea. A similar range for annually averaged primary productivity in the Ionian Sea ($74.3\text{--}418.8 \text{ mg C m}^{-2} \text{ day}^{-1}$) is suggested by the model simulations by Allen et al. (2002).

It is remarkable that the different physical conditions imposed in the two experiments do not cause substantial changes in the ecosystem structure and productivity.

The increased nutrient input in the experiments *Now 1* and *Holo 1* forces the ecosystem towards more productive conditions which are far from the present-day eastern Mediterranean conditions. In both experiments primary productivity is mostly concentrated in a short duration spring bloom (Fig. 8C, D) and decreases considerably during the rest of the

Table 3

Primary productivity in the euphotic zone ($\text{mg C m}^{-2} \text{ day}^{-1}$) and organic carbon fluxes at 500 m and at the bottom ($\text{mg C m}^{-2} \text{ day}^{-1}$) for the different simulations

Experiment	Primary productivity ($\text{mg C m}^{-2} \text{ day}^{-1}$)	POC flux at 500 m ($\text{mg C m}^{-2} \text{ day}^{-1}$)	POC flux at the bottom ($\text{mg C m}^{-2} \text{ day}^{-1}$)
Now Low	125	1.4	—
Now 1	575	4.7	—
Now 2	2420	11.5	—
Holo Low	125	1.4	—
Holo 1	440	7.2	—
Holo 2	1995	16.5	14.7

All the values are mediated over the last 100 years of integration.

year. The peak in productivity corresponds to the formation of a spring DCM located at 140 m (Fig. 7C,D) where concentrations reach the values of about $0.8 \text{ mg chl-a m}^{-3}$ for *Now 1* and $0.5 \text{ mg chl-a m}^{-3}$ for *Holo 1*. The dominant group in the DCM is again picophytoplankton, while phytoflagellates represent a minor fraction of the primary producers and grow in surface and sub-surface waters; diatoms have very low biomasses. Maximum pelagic bacteria biomass develops in correspondence to the DCM exploiting dissolved and particulate organic carbon produced by phytoplankton. In both experiments microzooplankton is present in surface waters, feeding on phytoflagellates; zooflagellates develop in correspondence to the DCM grazing on picophytoplankton and bacteria. On the whole, biomasses and primary productivity are slightly higher in the *Now 1* experiment with respect to *Holo 1*.

Experiments *Now 2* and *Holo 2* yielded an ecosystem structure characterized by peak productivities concentrated in a DCM located at about 70 m depth during spring (Fig. 7E,F). However, primary productivity shows high values throughout the whole year (Fig. 8E,F). In both simulations about 70% of the total phytoplankton biomass is constituted by picophytoplankton and the remaining 30% by autotrophic flagellates. Both groups bloom at the same depth in the water column; the same distribution characterizes zooplankton and pelagic bacteria whose aggregate biomasses are higher in the experiment *Now 2*.

Primary productivity estimates for the time of deposition of the sapropel S1 suggest a range of 5 to 10 times present-day productivities in the eastern Mediterranean (Howell and Thunnell, 1992; Strohle and Krom, 1997); a slightly lower estimate (around $320 \text{ mg C m}^{-2} \text{ day}^{-1}$) is suggested by Passier et al. (1999a,b). A similar range of variability is indicated by several authors for sapropels deposited in the

eastern Mediterranean during the Pliocene and Quaternary (Passier et al., 1999a,b; Wehausen and Brumsack, 1999; Weldeab et al., 2003). The productivity simulated in *Holo 1* falls within the suggested range, while the productivity of *Holo 2* appears overestimated compared to the data. Both simulated ecosystems show productivities concentrated in a DCM, as suggested by several authors for the sapropel deposition time. *Holo 1* is more influenced by seasons, while *Holo 2* appears to have a persistent primary productivity during the whole year.

3.2. Dissolved oxygen and organic carbon deposition

The oxygen concentration in the water column depends on the interplay among surface input, vertical/horizontal advection and diffusion, primary production and bacteria (pelagic and benthic) respiration. The 2000-year evolution of the oxygen concentration in the water column for all the experiments is shown in Fig. 9.

The simulations under present-day physical conditions with lateral ventilation involving the whole extension of the water column show no substantial variations of the oxygen concentration, regardless of the surface primary productivity. In the *Holo Low* experiment, where oxygen horizontal advection is suppressed below 500 m depth, oxygen consumption due to POM remineralization by bacteria induces the formation of a strongly dysoxic zone (with oxygen concentrations not lower than 10 mmol m^{-3}) that at the end of the simulation involves depth comprised between 500 and 800 m (Fig. 9B).

The more productive experiments *Holo 1* and *Holo 2* show the formation and expansion towards the bottom of an anoxic zone where oxygen concentrations drop under the threshold concentration of 4.5 mmol m^{-3} , assumed as the upper limit for anoxic conditions (Cramp and O'Sullivan, 1999). Anoxia develops first under the reventilated layer at a depth of 550–600 m, after 390 years from the beginning of the simulation for *Holo 1* and 320 years for *Holo 2*, and subsequently expands downwards at a rate related to the magnitude of the particulate organic carbon fall-out from the reventilated layers (500 m, see Table 3). The velocity of the anoxic front is about 75 m every 100 years for *Holo 1* and 130 m every 100 years for *Holo 2*. The dynamics of evolution of the anoxic conditions is the same as suggested by Strohle and Krom (1997), and simulated for the weakened anti-estuarine circulation scenario by Stratford et al.

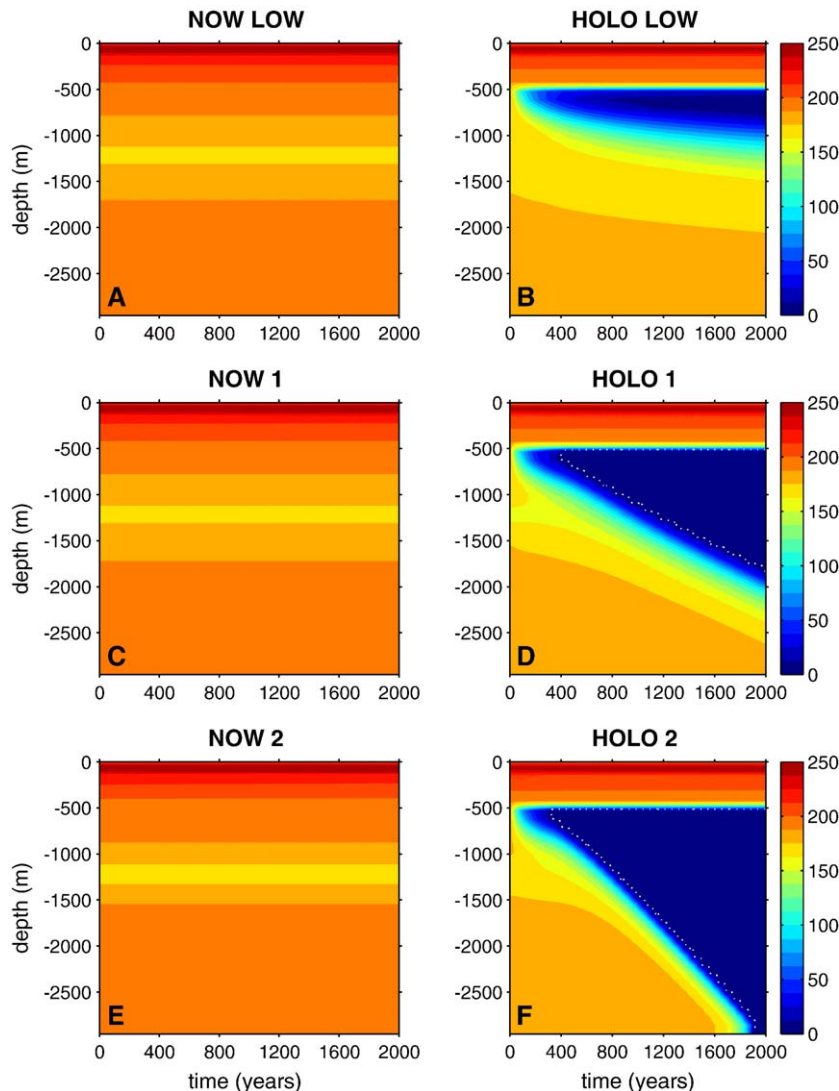


Fig. 9. Dissolved oxygen concentrations for the 2000 years simulation time of the NOW and HOLO experiments. Units are mmol m^{-3} . The upper limit of anoxic conditions (4.5 mmol m^{-3} , after Cramp and O'Sullivan, 1999) is marked by the white dotted line.

(2000); the velocities are respectively about 7 and 4 times lower in our simulations.

The capability of the pelagic bacteria to consume oxygen by decomposing the settling organic detritus produced in the surface layers appears central in controlling the ‘top-to-bottom’ progress of the oxygen depletion’ (Strohle and Krom, 1997). The remineralization process is so efficient that detritus is completely exhausted while settling through the water column, determining the formation under the reventilated layers of a minimum in oxygen concentration where anoxic conditions are reached. The onset of anoxia in the deep layers appears central in allowing organic carbon to accumulate into the sediments. Only when

anoxic conditions are established at the seafloor organic carbon can deposit and be preserved in the sediments. At the end of the 2000 simulated years no organic carbon deposition is observed at the bottom under an oxygenated water column and relatively low primary productivity; the *Holo 2* experiment alone shows anoxic waters at the sediment/water interface and organic carbon flux to the bottom of $14.7 \text{ mg C m}^{-2} \text{ day}^{-1}$ (Table 3).

Estimated organic carbon depositional fluxes at the seafloor for sapropel S1 times deduced from the geochemical characteristics of the sedimentary record indicate a similarity with the values compiled in Table 3. Slomp et al. (2004) suggest a value of 7.2 mg C m^{-2}

Table 4

Sensitivity experiments to the settling velocity of particulate organic matter

Experiment	Physical conditions and oxygen reventilation	Surface nutrients	Settling velocity for particulate organic matter (m day^{-1})
H1-V1	Holocene	Reconstruction 1	5.0
H1-V2	Holocene	Reconstruction 1	10.0
H2-V1	Holocene	Reconstruction 2	5.0
H2-V2	Holocene	Reconstruction 2	10.0

day^{-1} , Calvert et al. (1992) a value of $6.6 \text{ mg C m}^{-2} \text{ day}^{-1}$; a higher estimate, provided by Howell and Thunnell (1992), is approximately $33 \text{ mg C m}^{-2} \text{ day}^{-1}$. The model results by Stratford et al. (2000) for open sea locations are closer to the lower estimates ($6.6 \text{ mg C m}^{-2} \text{ day}^{-1}$).

3.3. Sensitivity experiments to the settling velocity of the particulate organic matter

The settling velocity of the particulate organic detritus produced in the euphotic zone is a critical parameter in determining the magnitude of the primary productivity and POM fluxes in the water column (Boyd and Newton, 1999; Druon and Le Fèvre, 1999) and the development and maintenance of the DCM (Hodges and Rudnick, 2004). This parameter is set in our model at the constant value of 1.5 m day^{-1} , but it is suggested that under increased productivity conditions, or in the presence of processes able to enhance particle aggregation, this value could be underestimated. Aggregation of heterogeneous organic particles appears to have a remarkable importance in the surface layers (50–100 m) of oceanic regions (Boyd et al., 1999). Mucous

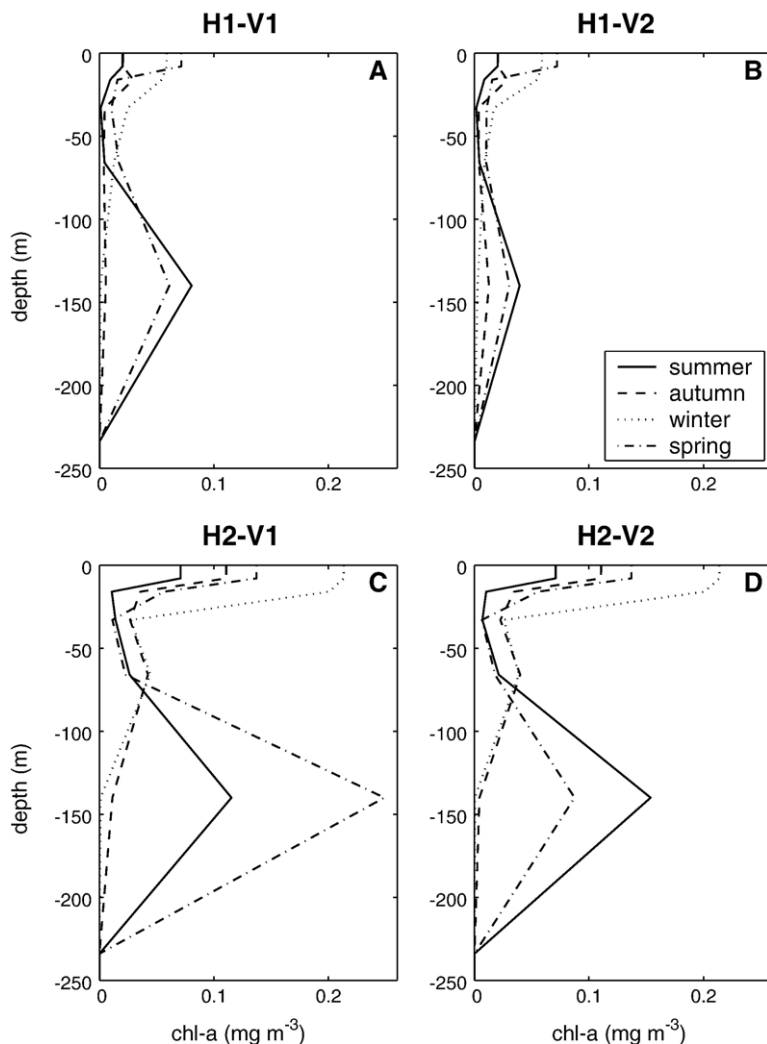


Fig. 10. Seasonal chlorophyll-a profiles for the sensitivity experiments. Units are mg m^{-3} .

aggregates constituted by faecal pellets, fresh siliceous and carbonate matter, entire and fragmented phytoplanktonic and zooplanktonic cells characterize the material caught by sediment traps in the Ionian Sea (Boldrin et al., 2002); in this area the estimated sinking speed is greater than 140 m day^{-1} , in the range of the settling velocities of faecal pellets and large cell aggregates. The model setup by Stratford et al. (2000) parameterized sedimentation processes with a settling velocity for organic detritus of 200 m day^{-1} , using the estimate in the range of 100 and 200 m day^{-1} reported for the sedimentation of oceanic phytodetritus after large phytoplanktonic bloom episodes (Honjo and Manganini, 1993; Honjo et al., 1995; Smith et al., 1996). For the NW Mediterranean Harris et al. (2001) suggest a vertical organic carbon (both dissolved and particulate) flux in the range of $5\text{--}10 \text{ m day}^{-1}$.

The experiments *Holo 1* and *Holo 2* are characterized by higher productivities than *Holo Low* and by the increased importance of larger phytoplankton within the food-web. Even if the largest model functional groups such as mesozooplankton and diatoms do not increase their abundance in the two experiments a legitimate question can be raised about the consequences of a possible increase of detritus size, and consequently sinking rate, on carbon fluxes and oxygen content in the water column. To get more insight into this issue, four additional experiments (Table 4) have

been setup retaining the characteristics of the *Holo 1* and *Holo 2* experiments and increasing the settling velocity of the POM from the original value of 1.5 m day^{-1} to the values of 5.0 and 10.0 m day^{-1} .

Choosing these two values we took into account that the value of the sinking velocity must be representative of a spectrum of particles ranging from sinking pico-, nano- and microphytoplanktonic dead cells (velocities in the range of $0\text{--}8 \text{ m day}^{-1}$, with the higher estimate valid for large diatom cells, Druon and Le Fèvre, 1999) and dead zooplankton and faecal pellets or other aggregates (velocity estimates between 10 and 300 m day^{-1} , with the upper range suitable to mesozooplankton faecal pellets, Druon and Le Fèvre, 1999). Velocities higher than 10 m day^{-1} were not used since the highest estimates did not seem appropriate to parameterize the velocity of all the particulate material produced by an ecosystem dominated by low-dimension phyto- and zooplanktonic groups as happens in our model. In addition the ecosystem simulations made with POM sinking velocities of the order of $50\text{--}100 \text{ m day}^{-1}$ yielded unrealistic results.

Figs. 10 and 11 show the seasonal profiles of chlorophyll-a and the seasonal cycle of the euphotic zone vertically integrated net primary productivity for the four sensitivity experiments; Table 5 shows the annual mean integrated primary productivities and annual mean organic carbon sedimentation fluxes at the depth of 500 m and at the bottom. As for the other

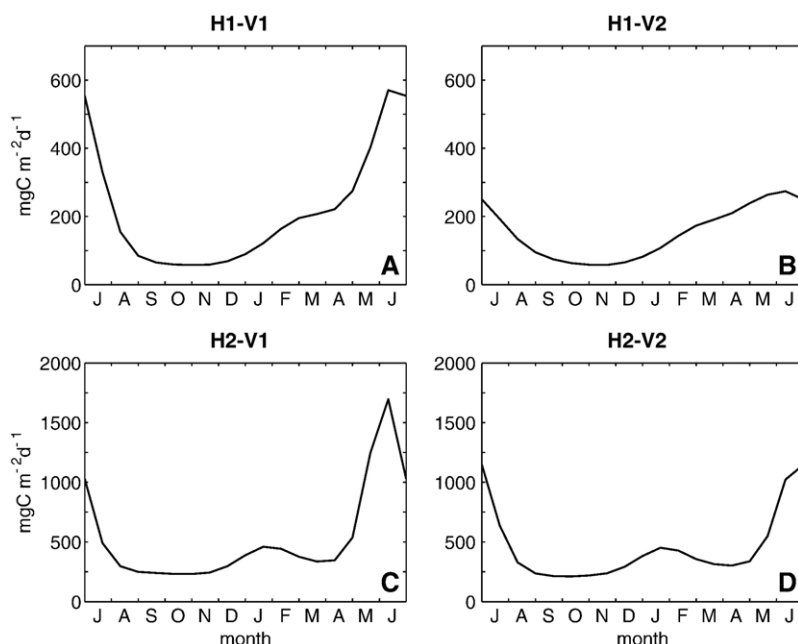


Fig. 11. Vertically integrated net primary productivities for the sensitivity experiments. Units are $\text{mg C m}^{-2} \text{ day}^{-1}$.

Table 5

Primary productivity in the euphotic zone ($\text{mg C m}^{-2} \text{ day}^{-1}$) and organic carbon fluxes at 500 m and at the bottom ($\text{mg C m}^{-2} \text{ day}^{-1}$) for the sensitivity experiments to the settling velocity

Experiment	Primary productivity ($\text{mg C m}^{-2} \text{ day}^{-1}$)	POC flux at 500 m ($\text{mg C m}^{-2} \text{ day}^{-1}$)	POC flux at the bottom ($\text{mg C m}^{-2} \text{ day}^{-1}$)
H1-V1	205	9.8	2.4
H1-V2	150	9.5	2.9
H2-V1	510	25.3	25.3
H2-V2	430	27.6	27.4

All the values are mediated over the last 100 years of integration.

simulations, the results are averaged over the last 100 years of integration.

An immediate consequence of the increased POM settling velocity is a shift of the ecosystem towards less productive conditions, as shown by chlorophyll-a profiles and productivities. In all the experiments phytoplankton biomass is clearly divided between surface waters, where autotrophic flagellates bloom during winter and spring months, and a DCM situated at the base

of the euphotic zone originated by picophytoplankton blooming during spring and summer. Productivities decrease as the settling velocity increases (Fig. 10 and Table 5), due to the more effective removal of nutrient from the shallow euphotic zone by the fast-sinking POM. The nutrients are in fact upwelled after remineralization by bacteria and this process is not so efficient if sinking velocities are high.

The model productivities simulated in the experiments H2-V1 and H2-V2 are closer to the lower estimates for sapropel S1 times (roughly 5 times the present-day productivity) while for the experiments H1-V1 and H1-V2 the model provides even lower values, intermediate between present-day productivities and the lower estimates for S1. At the same time the particulate organic carbon flux due to sedimentation increases to 9.3 and 9.8 $\text{mg C m}^{-2} \text{ day}^{-1}$ for experiments H1-V1 and H1-V2 and to 25.3 and 27.6 $\text{mg C m}^{-2} \text{ day}^{-1}$ for H2-V1 and H2-V2 at the depth of approximately 500 m (Table 5). In all the sensitivity experiments a significant fraction of the sinking POM is not remineralized in the water column and reaches the

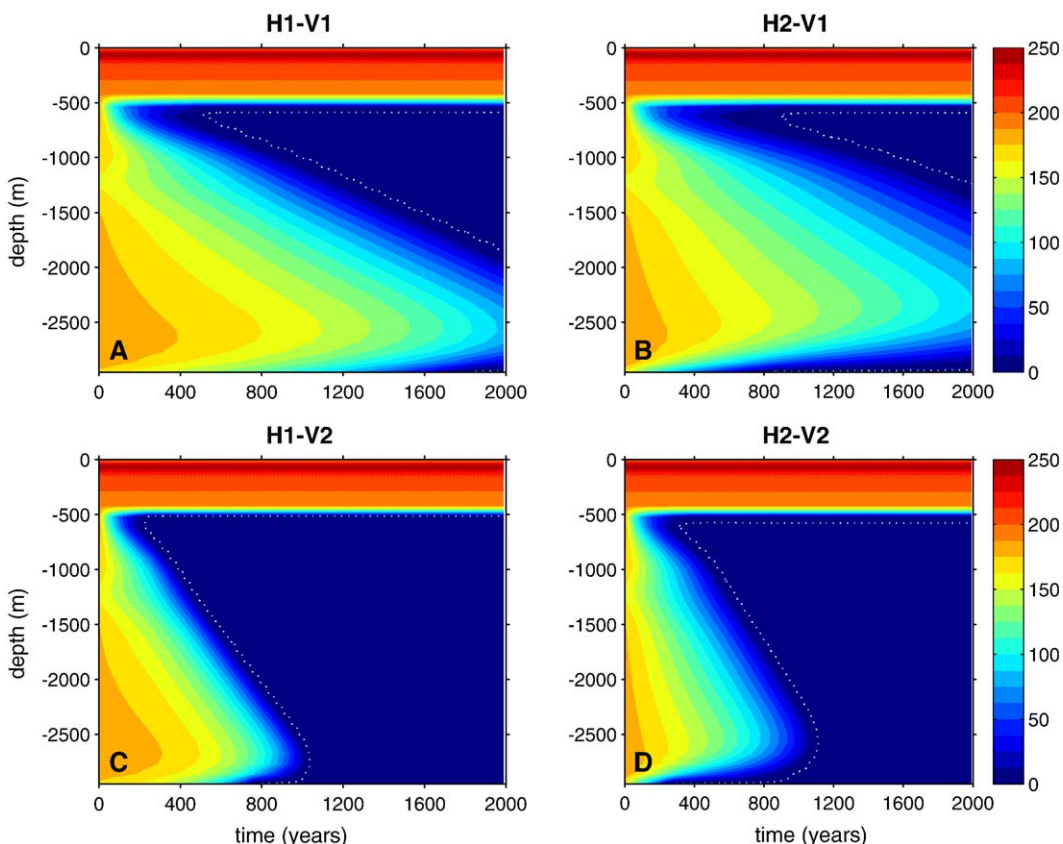


Fig. 12. Dissolved oxygen concentrations for the 2000 years simulation time for the sensitivity experiments. Units are mmol m^{-3} . The upper limit of anoxic conditions (4.5 mmol m^{-3} , after Cramp and O'Sullivan, 1999) is marked by the white dotted line.

sediments where it accumulates and triggers sediment and bottom-water anoxia, as shown in Fig. 12. These experiments thus display the combined onset of anoxic condition below the ventilation depth and at the sediment/water interface; anoxia is reached at 600 m depth after 510, 890, 220 and 310 years, and at the bottom after 1820, 820, 770 and 280 years for the four experiments respectively. When the POM settling velocity is set at the highest value the onset of anoxia is roughly simultaneous at 600 m and at the bottom (Fig. 12C and D). In all the cases the onset of anoxic conditions at the seafloor originates in a thin layer confined near the bottom in a similar way as suggested by Casford et al. (2003). The organic carbon fluxes to the seafloor at the end of the simulations are reported in Table 5. The experiments *H1-V1* and *H2-V1* produce sedimentation fluxes of 2.4 and 2.9 mg C m⁻² day⁻¹ respectively, lower than the estimates for sapropel S1 reported in Section 3.1. Nevertheless, the magnitude of such fluxes, in the last simulated century, increases, approaching the 500 m depth value, as the water column becomes completely anoxic. Organic carbon sedimentation in the experiments *H2-V1* and *H2-V2* (of 25.3 and 27.4 mg C m⁻² day⁻¹) is closer to the higher estimates for S1.

The establishment of anoxic conditions in H2-V2 shows another important change with respect to the *Holo 2* experiment. The timescale for the bottom anoxia is only 280 years (Fig. 12D) instead of 1900 (Fig. 9F). This is more consistent with the timescale of anoxic conditions established after the interruption of 200 years during S1 (Rohling et al., 1997; De Rijk et al., 1999). Thus H2-V2 seems to be the more realistic experiment in terms of timescale.

4. Discussion and conclusions

Sapropel deposition has been linked to a shift in the thermohaline circulation of the eastern Mediterranean Sea and an increase in surface primary productivity driven by an enhanced nutrient input in the euphotic zone. By coupling a one-dimensional physical model and an ecosystem model we tried to simulate the biogeochemical conditions that led to sapropel deposition. Although we use a reconstruction of the water column physical conditions taken from a simulation of the Holocene the main results can be applied to the sapropel topic in general.

A first result is the low sensitivity of the ecosystem, under present-day nutrient input, to the different water stratification assumed for the Holocene. The experiments *Now Low* and *Holo Low* show in fact an almost

identical ecosystem structure, without the (supposed) increase in productivity induced by a stronger stratification during the Holocene. Furthermore the comparison between the simulations *Now 1* and *Holo 1* and *Now 2* and *Holo 2* indicates that present-day physical conditions by themselves allow a higher productivity once assigned increased nutrient surface concentrations. At the same time the interruption of the deep oxygenation, due to the reduced extension of the vertical thermohaline circulation cell during the Holocene (Myers et al., 1998), appears essential in the paleosimulations to allow anoxia and give rise to significant organic carbon fluxes to the sediments.

Sapropel deposition appears necessarily linked to an increase in nutrient supply: even suppressing the reventilation of deep water masses, a present-day like ecosystem (*Holo Low* experiment) is not able to sustain organic carbon sedimentation and accumulation at the seafloor; in this case only a strongly dysoxic zone is observed at mid-depths but true anoxic conditions are not reached and sedimentation of organic matter at the seafloor does not take place. Organic carbon deposition is observed when increased nutrient concentrations in the upper layers enhance primary productivity and, consequently, POM production and sedimentation through the water column. The increased flux, together with the lack of lateral ventilation, determines oxygen consumption in the intermediate and deep layers and the deposition of organic carbon at the seafloor; the preservation of the organic matter in the sediments is allowed by the anoxic environmental conditions.

When the POM settling velocity is low (1.5 m day⁻¹ in the experiments *Holo 1* and *Holo 2*) the remineralization activity of pelagic bacteria can exhaust the whole supply of detritus while it is still sinking in the oxygenated water column. In this case dysoxic and subsequently anoxic conditions develop under the reventilation depth and expand downwards while the oxygen reservoir is gradually eroded; finally, organic carbon sedimentation is made possible when anoxic conditions reach the bottom. The timescale of the downward expansion of the anoxic zone appears controlled mainly by the magnitude of the organic carbon flux that leaves the ventilated layer. The capability of pelagic bacteria to remineralize efficiently the organic carbon settling through the oxygenated water column implies that a source of organic matter concentrated in a pronounced and deep chlorophyll maximum can support higher carbon fluxes to the deep stagnating water masses than a shallow source, inducing faster onset of anoxic conditions and sapropel deposition.

Possible processes able to increase the sedimentation velocity of POM (i.e., increase in size of the sinking particles and aggregation processes) determine a redistribution of nutrients in the euphotic zone and the rearrangement of the ecosystem structure, and support the growth of a productive DCM at the base of the euphotic zone. The deepening of the DCM is evident comparing experiment *Holo 2* (Fig. 7) with the experiments *H2-V1* and *H2-V2* (Fig. 10c and d respectively). As the sedimentation velocity of organic detritus increases we observe the concomitant decrease in primary productivity and the enhancement of the POM fluxes at the reventilation depth under the same surface nutrient conditions (Table 5). Due to the enhanced efficiency in the export of POM the less productive ecosystems simulated in *H1-V1*, *H1-V2* and *H2-V1*, *H2-V2*, produce higher particulate fluxes than the more productive ones in *Holo 1* and *Holo 2*. As a consequence the increase in the sinking velocity also affects the dynamics of anoxia and deep sedimentation. The higher efficiency of the POM posting mechanism allows part of this detritus to escape remineralization in the water column and reach the bottom while deep waters are still oxygenated. Here organic matter deposition determines progressively low oxygen/dysoxic environment, before full anoxic conditions are reached. When anoxia develops it remains confined in a narrow layer ('anoxic blanket') near the seafloor, appearing earlier than the development of a fully anoxic water column, until the downward propagating anoxic front originated under the reventilation depth reaches the deep layers.

The occurrence of a short scale (200-year) S1 interruption linked to the re-establishment of deep water ventilation (Rohling et al., 1997; De Rijk et al., 1999) suggests that the onset of anoxic conditions could have followed a pattern similar to the one obtained by using an increased sedimentation velocity. In fact, assuming that the sapropel interruption testifies an episode of re-oxygenation of the water column, the simulation with increased nutrient supply and enhanced POM sedimentation velocity (*H2-V2*) appears better to match the timescales for the onset of anoxic conditions at the sea bottom for the whole water column during the S1 interruption event.

Our simulations document the relatively fast development of an anoxic blanket at the seafloor, related to the rapid POM posting mechanism, whereas the water column remains partially oxygenated. In our opinion this seafloor anoxic blanket suggested by Casford et al. (2003) could better explain the conditions under which the sapropel S1 was realized in the eastern Mediterranean due to the faster timescales.

In conclusion we believe this study has shown for the first time that S1 deposition occurred by the concomitant effect of absent reventilation and enhanced productivity with the additional contribution of large POM sinking velocity. Thus the quality of the sinking material and the thermohaline circulation characteristics are necessary and sufficient conditions for the high organic material burial rates. Our paper opens new research needs about S1 deposition: (1) identification of the paleo-sources of nutrients that triggered the larger productivity during sapropel deposition, (2) a detailed understanding of the functioning of the paleo-trophic web, (3) a deeper insight on the role of the organic matter aggregation processes.

Acknowledgments

We are greatly indebted to P. Myers for making available to us the results of his Mediterranean Sea Holocene paleosimulations. Additional thanks are also due to Francesca Sangiorgi for frequent and useful discussions. This work was supported by the Italian Ministry of University and Scientific-Technological Research under the PRIN Program and the SINAPSI Project.

Appendix A

A.1. Physical one-dimensional model

The 1-D version of the Princeton Ocean Model computes the tracers, temperature and salinity, the velocity components and the vertical viscosity and diffusivity profiles. In this model adaptation, vertical temperature and salinity profiles are imposed from the model simulations of Myers et al. (1998). The velocity components profiles are used only as input to calculate vertical shear for the turbulence closure submodel (Mellor and Yamada, 1982). These equations are written for the turbulent kinematic energy, b^2 , and the mixing length, b^2l , using the following equations:

$$\frac{\partial}{\partial t} \left(\frac{b^2}{2} \right) = \frac{\partial}{\partial z} \left(K_b \frac{\partial b^2/2}{\partial z} \right) + P_s + P_b - \epsilon \quad (\text{a.1})$$

$$\frac{\partial}{\partial t} (b^2 l) = \frac{\partial}{\partial z} \left(K_b \frac{\partial b^2 l}{\partial z} \right) + E_1 [P_s + P_b] - \frac{q^3}{B_1} \tilde{W} \quad (\text{a.2})$$

where K_b is the vertical turbulent diffusion coefficient for b^2 , \tilde{W} is a function of the distance from rigid boundaries, P_s is the turbulent kinetic energy production by shear, P_b is the buoyant production/dissipation,

ε is the dissipation according to Kolmogorov and B_1 , E_1 are empirical constants.

The vertical diffusivity coefficients are then calculated by assuming

$$K_H(z) = qIS_H \quad (a.3)$$

where S_H is a stability function calculated as function of a Richardson number and empirical constants.

The boundary conditions for turbulent kinetic energy at the surface depend on the wind stress intensity, and the form used here is:

$$q^2 = B_1^{2/3} \frac{|\bar{\tau}_w|}{c_d} \text{ at } z = 0 \quad (a.4)$$

where $\bar{\tau}_w = c_d |\bar{U}_{wind}|$ is the wind stress at the surface, c_d is the surface drag coefficient and \bar{U}_{wind} is the horizontal wind velocity at the surface.

In our simulations the Climatic Optimum wind stress was taken from Dong and Valdes (1995) and from Myers et al. (1998).

The boundary condition for the Eq. (a.1) at the bottom is:

$$q^2 = B_1^{2/3} \frac{|\bar{\tau}_b|}{c_b} \text{ at } z = -H \quad (a.5)$$

where $\bar{\tau}_b = c_b |\bar{U}(-H, t)|$ $\bar{U}(-H, t)$ is the stress at the bottom, c_b is the bottom drag coefficient and sub $\bar{U}(-H, t)$ is the horizontal velocity at the bottom.

A.2. Biogeochemical model equations

The ERSEM model computes the temporal rate of change of a generic biogeochemical variable A (expressed in terms of concentration) as:

$$\frac{\partial A}{\partial t} = \frac{\partial A}{\partial t} \Big|_{\text{phys}} + \frac{\partial A}{\partial t} \Big|_{\text{bio}} \quad (a.6)$$

where

$$\frac{\partial A}{\partial t} \Big|_{\text{phys}} = -(w_u + w_{\text{sink}}) \frac{\partial A}{\partial z} + \frac{\partial}{\partial z} \left[K_H \frac{\partial A}{\partial z} \right] \quad (a.7)$$

is the rate of change due to physical processes and $\frac{\partial A}{\partial t} \Big|_{\text{bio}}$ is the rate of change due to the biogeochemical interactions described by ERSEM equations. Here w_{sink} represents the settling velocity of the variable, if applicable, as in the case of particulate organic matter and diatoms. In addition w_u is an imposed vertical velocity in the domain parameterizing the effects of large scale upwelling on the dissolved constituents. w_u is different from zero only for dissolved nitrate, phosphate, ammonium, silicate and oxygen and is described later.

Eq. (a.6) is solved with an Euler forward time integration scheme; time step cutting is used when the integration produces negative concentrations. During time step cutting the physical rate of change $\frac{\partial A}{\partial t} \Big|_{\text{phys}}$ is held constant.

The initial conditions for Eq. (a.6) at time $t=0$ is:

$$A(z) \Big|_{t=0} = A_0(z) \quad (a.8)$$

where $A_0(z)$ is the initial profile of the variable A .

The boundary conditions for (a.6) are:

$$K_V \frac{\partial A}{\partial z} \Big|_{z=-H} = 0 \text{ at the surface } (z = 0) \quad (a.9)$$

and

$$K_V \frac{\partial A}{\partial z} \Big|_{z=-H} = 0 \text{ at the bottom } (z = -H). \quad (a.10)$$

Different boundary conditions are used for nutrients at the surface. For these state variables the nutrient concentration listed in Table 1 is imposed at the surface, i.e.:

$$A(t) \Big|_{z=0} = A_{\text{surf}}. \quad (a.11)$$

A.3. Bacterial dynamics and oxygen consumption

In the present study bacterial respiration is of primary importance for the onset of anoxic conditions in the aphotic zone. We provide here a brief summary of the ERSEM equations related to this aspect of bacterioplankton dynamics.

The temporal rate of change of bacterial carbon content (B_C) due to uptake from the dissolved and particulate detrital sources and to respiration is expressed by:

$$\frac{\partial B_C}{\partial t} = \frac{\partial B_C}{\partial t} \Big|_{\text{uptk}}^{\text{uptk}} - \frac{\partial B_C}{\partial t} \Big|_{\text{rsp}}^{\text{rsp}}. \quad (a.12)$$

Carbon uptake is given by

$$\frac{\partial B_C}{\partial t} \Big|_{\text{uptk}}^{\text{uptk}} = \min(G^{\text{sub}}, G^{\text{env}}) \quad (a.13)$$

where G^{sub} is the potential uptake due to the availability of both dissolved and particulate detritus and G^{env} is the potential uptake allowed by the environmental conditions. G^{env} is calculated as:

$$G^{\text{env}} = r_0 f_T f_{O_2} B_C \quad (a.14)$$

where r_0 is the maximum potential uptake of carbon as fraction of biomass modulated by non-dimensional regulating factors that are function of temperature(f_T) and oxygen concentration (f_{O_2}).

f_{O_2} is parameterized with a Michaelis-Menten formulation as:

$$f_{O_2} = \frac{O_2}{O_2 + O_2^*} \quad (\text{a.15})$$

where the dissolved oxygen concentration O_2 is considered, and O_2^* is the oxygen concentration at which metabolic functionalities are halved.

f_T is written in an exponential form as:

$$f_T = Q_{10}^{\frac{T-10}{10}} \quad (\text{a.16})$$

where Q_{10} is the characteristic temperature coefficient of bacteria and T is the temperature in °C.

Bacterial respiration (as well as respiration of all pelagic groups) determines an oxygen consumption expressed by the following equation:

$$\frac{\partial O_2}{\partial t} \Big|_{\text{rsp}} = -\theta \frac{\partial B_C}{\partial t} \Big|_{\text{rsp}}, \quad (\text{a.17})$$

where θ is the conversion coefficient between carbon respired and oxygen consumed.

A.4. Vertical velocity for dissolved components: open sea upwelling

The Ionian Basin area that comprises the area of implementation of the model is subject to a wind system that can determine large scale upwelling/downwelling phenomena owing to the wind stress curl (Ekman pumping), described by the equation:

$$w_u = \hat{k} \cdot \vec{\nabla} \times \left(\frac{\vec{\tau}_w}{\rho f} \right) \quad (\text{a.18})$$

where w_u is the vertical velocity, $\vec{\tau}_w$ is the wind stress, ρ is the seawater density and f is the Coriolis parameter. The order of magnitude of the vertical velocity (w_{\max}) can be estimated by means of a scale analysis of the former equation.

$$w_{\max} = O[w_u] = \frac{\tau_0}{L \rho_0 f_0} \quad (\text{a.19})$$

where we chose the significant values: $\tau_0 = 1 \text{ dyn cm}^{-2}$, $\rho_0 = 1 \text{ g cm}^{-3}$ and $f_0 = 10^{-4} \text{ s}^{-1}$ for the wind stress, density and Coriolis parameter, and $L = 500 \text{ km}$.

By a substitution of the chosen values in the equation we get the order of magnitude of w_{\max} , equal to $10^{-4} \text{ cm s}^{-1}$. This value can be considered an upper limit for the wind-induced vertical velocity. By knowing the sign of the wind stress curl in the area of study (Pinardi and Navarra, 1993) we can assume w_{\max} as positive and therefore defining upwelling processes.

We introduced in the model a vertical upwelling velocity for the dissolved components, varying in depth and time. The maximum value of this velocity has been chosen equal to the half of w_{\max} and is reached during the winter months, when wind stress is highest according to observations. During late summer months this value is reduced by a factor of 10. Fig. A.1 shows the upwelling velocity profile during the winter maximum and the summer minimum.

A.5. Oxygen lateral advection parameterization

In the deep parts of the Mediterranean Sea, far from deep-water formation zones, oxygen is supplied mostly by lateral advection processes.

To simulate the input of oxygen by horizontal advection we introduced in the model a linear relaxation term in the ERSEM prognostic equation for the dissolved oxygen:

$$\frac{\partial O_2}{\partial t} = \frac{\partial O_2}{\partial t} \Big|_{\text{phys}} + \frac{\partial O_2}{\partial t} \Big|_{\text{bio}} + \frac{\partial O_2}{\partial t} \Big|_{\text{relax}} \quad (\text{a.20})$$

with

$$\frac{\partial O_2(t)}{\partial t} \Big|_{\text{relax}} = -r [O_2(t) - O_2^{\text{init}}] \quad (\text{a.21})$$

where O_2^{init} is the initial (present-day) oxygen profile and r is the relaxation coefficient, whose inverse rep-

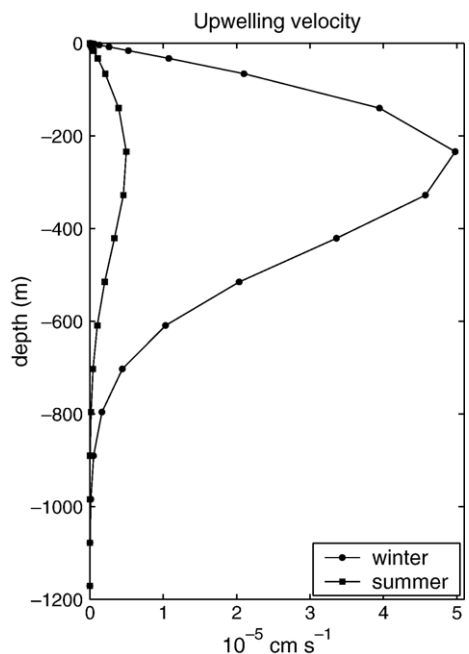


Fig. A.1. Vertical profiles of the upwelling vertical velocity for summer and winter. Units are $10^{-5} \text{ cm s}^{-1}$.

resent the temporal scale of the oxygen advection processes and is set equal to 30 days. The effect of this equation is to drive the oxygen concentration towards the values expressed by the initial condition. The oxygen profile correction is applied to the whole water column in the present-day simulations, in order to model the water mass oxygenation actually observed in the eastern Mediterranean Sea, and from the surface to a depth of about 500 m for the simulations of the Climatic Optimum, according to the results of Myers et al. (1998).

References

- Allen, J.I., Blackford, J.C., Radford, P.J., 1998. An 1-D vertically resolved modelling study of the ecosystem dynamics of the middle and southern Adriatic Sea. *Journal of Marine Systems* 18, 265–286.
- Allen, J.I., Somerfield, P.J., Siddorn, J., 2002. Primary and bacterial production in the Mediterranean Sea: a modeling study. *Journal of Marine Systems* 33–34, 473–495.
- Baretta, J.W., Ebenhoh, W., Ruardij, P., 1995. The European Regional Seas Ecosystem Model, a complex marine ecosystem model. *Netherlands Journal of Sea Research* 33 (3/4), 233–246.
- Baretta-Bekker, J., Baretta, J., Rasmussen, E., 1995. The microbial food web in the European Regional Seas Ecosystem Model. *Netherlands Journal of Sea Research* 33 (3/4), 363–379.
- Bethoux, J.P., 1989. Oxygen consumption, new production, vertical advection and environmental evolution in the Mediterranean Sea. *Deep-Sea Research* 36, 769–781.
- Blumberg, A.F., Mellor, G.L., 1987. A description of a three dimensional coastal ocean circulation model. In: Heaps, N.S. (Ed.), *Three Dimensional Coastal Ocean Models*. AGU, pp. 1–16.
- Boldrin, A., Misericordi, S., Rabitti, S., Turchetto, M.M., Balboni, V., Soccal, G., 2002. Particulate matter in the southern Adriatic and Ionian Sea: characterisation and downward fluxes. *Journal of Marine Systems* 33–34, 389–410.
- Bosch, H.-J., Sinninghe Damsté, J.S., de Leeuw, J.W., 1998. Molecular paleontology of Eastern Mediterranean sapropels: evidence for photic zone anoxia. In: Robertson, A.H.F., Emeis, K.-C., Richter, C., Camerlenghi, A. (Eds.), *Proc. ODP Sci. Res.*, vol. 160. Ocean Drilling Program, College Station, TX, pp. 285–295.
- Boyd, P.W., Newton, P.P., 1999. Does planktonic community structure determine downward particulate organic carbon flux in different oceanic provinces? *Deep Sea Research I* 46, 63–91.
- Boyd, P.W., Sherry, N.D., Berge, J.A., Bishop, J.K.B., Calvert, S.E., Charette, M.A., Giovannoni, S.J., Goldblatt, R., Harrison, P.J., Moran, S.B., Roy, S., Soon, M., Strom, S., Thibault, D., Vergin, K.L., Whitney, F.A., Wong, C.S., 1999. Transformations of biogenic particulates from the pelagic to the deep ocean realm. *Deep Sea Research II* 46, 2761–2792.
- Bregant, D., Catalano, C., Civitarese, G., Luchetta, A., 1990. Some characteristics of the brines in Bannock and Tyro Basins: salinity, sulphur compounds, Ca, F, pH, At, PO₄, SiO₂, NH₃. *Marine Chemistry* 31, 35–62.
- Broekhuizen, N.R., Heath, M.R., Hay, S.J., Gurney, W.S.C., 1995. Modelling the dynamics of the North Seas mesozooplankton. *Netherlands Journal of Sea Research* 33 (3/4), 381–406.
- Calvert, S.E., 1983. Geochemistry of Pleistocene sapropels and associated sediments from the eastern Mediterranean. *Oceanologica Acta* 6, 255–267.
- Calvert, S.E., Nielsen, B., Fontugne, M.R., 1992. Evidence from nitrogen isotope ratios for enhanced productivity during formation of eastern Mediterranean sapropels. *Nature* 359, 223–225.
- Casford, J.S.L., Rohling, E.J., Abu-Zied, R.H., Fontanier, C., Jorisson, F., Leng, J., Schmiedl, M.J., Thomson, G., 2003. A dynamic concept for eastern Mediterranean circulation and oxygenation during sapropel formation. *Palaeogeography, Palaeoclimatology, Palaeoecology* 190, 103–119.
- Casotti, R., Landolfi, A., Brunet, C., D'Ortenzio, F., Mangoni, O., Ribera D'Alcalà, M., 2003. Composition and dynamics of the phytoplankton of the Ionian Sea (eastern Mediterranean). *Journal of Geophysical Research* 108 (PBE 17-1/17-19).
- Castradori, D., 1993. Calcareous nannofossils and the origin of eastern Mediterranean sapropels. *Paleoceanography* 8, 459–472.
- Cita, M.B., Vergnaud-Grazzini, C., Robert, C., Chamley, H., Ciaranfi, N., D'Onofrio, S., 1977. Paleoclimatic record of a long deep sea core from the eastern Mediterranean. *Quaternary Research* 8, 205–235.
- Cramp, A., O'Sullivan, G., 1999. Neogene sapropel in the Mediterranean: a review. *Marine Geology* 153, 11–28.
- Da Silva, A.M., Young, C.C., Levitus, S., 1995. Atlas of surface marine data. NOAA Atlas NESDIS, 7.
- De Rijk, S., Hayes, A., Rohling, E.J., 1999. Eastern Mediterranean sapropel S1 interruption: an expression of the onset of climatic deterioration around 7 ka BP. *Marine Geology* 153, 337–343.
- Dong, B., Valdes, P.J., 1995. Sensitivity studies of northern hemisphere glaciation using an atmosphere GCM. *Journal of Climate* 8, 2471–2496.
- Druon, J.N., Le Fèvre, J.L., 1999. Sensitivity of a pelagic ecosystem model to variations of process parameters within a realistic range. *Journal of Marine Systems* 19, 1–26.
- Ebenhoh, W., Kohlmier, C., Radford, P., 1995. The benthic biological submodel in the European Regional Seas Ecosystem Model. *Netherlands Journal of Sea Research* 33 (3/4), 423–452.
- Ediger, D., Yilmaz, A., 1996. Characteristics of deep chlorophyll maximum in the Northeastern Mediterranean with respect to environmental conditions. *Journal of Marine Systems* 9, 291–303.
- Emeis, K.-C., Sakamoto, T., Wehausen, R., Brumsack, H.-J., 2000. The sapropel record of the eastern Mediterranean Sea—results of Ocean Drilling Program Leg 160. *Palaeogeography, Palaeoclimatology, Palaeoecology* 158, 371–395.
- Harris, J.R.W., Stutt, E.D., Turley, C.M., 2001. Carbon flux in the northwest Mediterranean estimated from microbial production. *Deep-Sea Research I* 48, 2631–2644.
- Hartnett, H.E., Keil, R.G., Hedges, J.I., Devol, A.H., 1998. Influence of oxygen exposure time on organic carbon preservation in continental margin sediments. *Nature* 391, 572–574.
- Hilgen, F.J., 1991. Astronomical calibration of Gauss to Matuyama sapropels in the Mediterranean and implication for the Geomagnetic Polarity Time Scale. *Earth and Planetary Science Letters* 104, 226–244.
- Hodges, B.A., Rudnick, D.L., 2004. Simple models of steady deep maxima in chlorophyll and biomass. *Deep-Sea Research I* 51, 999–1015.
- Honjo, S., Manganini, S.J., 1993. Annual biogenic particle fluxes to the interior of the North Atlantic Ocean; studied at 34°N 21°W and 48°N 21°W. *Deep-Sea Research II* 40, 587–607.

- Honjo, S., Dymond, J., Collier, R., Manganini, S.J., 1995. Export production of particles to the interior of the equatorial Pacific Ocean during the 1992 EqPac experiment. *Deep-Sea Research Part II* 42, 831–870.
- Howell, M.W., Thunnell, R.C., 1992. Organic carbon accumulation in Bannock Basin: evaluating the role of productivity in the formation of eastern Mediterranean sapropels. *Marine Geology* 103, 461–471.
- Ignatiades, L., Psarra, S., Zervakis, V., Pagou, K., Souvermezoglou, E., Assimakopoulou, G., Gotsis-Skretas, O., 2002. Phytoplankton size-based dynamics in the Aegean Sea (Eastern Mediterranean). *Journal of Marine Systems* 36, 11–28.
- Jorissen, F.J., 1999. Benthic foraminiferal succession across Late Quaternary Mediterranean sapropels. *Marine Geology* 153, 91–101.
- Kallel, N., Paterne, M., Duplessy, J., Vergnaud-Grazzini, C., Pujol, C., Labeyrie, L., Arnold, M., Fontugne, M.R., Pierre, C., 1997. Enhanced rainfall in the Mediterranean region during the last sapropel event. *Oceanologica Acta* 20, 697–712.
- Kemp, A.E.S., Pearce, R.B., Koizumi, I., Pike, J., Rance, S.J., 1999. The role of mat-forming diatoms in the formation of Mediterranean sapropels. *Nature* 398, 57–61.
- Kidd, R.B., Cita, M.B., Ryan, W.B.F., 1978. Stratigraphy of eastern Mediterranean sapropel sequences recovered during DSDP Leg 42A and their paleoenvironmental significance. *Initial Reports of the Deep Sea Drilling Project* 42, 421–443.
- Krom, M.D., Michard, A., Cliff, R., Strohle, A., 1999. Source of sediments to the Ionian Sea and western Levantine basin of the eastern Mediterranean during S-1 sapropel times. *Marine Geology* 160, 45–61.
- Kroon, D., Alexander, I., Little, M., Lourens, L.J., Matthewson, A., Robertson, A.H.F., Sakamoto, T., 1998. Oxygen isotope and sapropel stratigraphy in the eastern Mediterranean during the last 3.2 million years. *Proceedings of the Ocean Drilling Program, Scientific Results* 160, 181–189.
- Larrasoña, J.C., Roberts, A.P., Rohling, E.J., Winklhofer, M., Wehausen, R., 2003. Three million years of monsoon variability over the northern Sahara. *Climate Dynamics* 21, 689–698.
- Li, W.K.W., Suba-Rao, D.V., Harrison, W.G., Smith, J.C., Cullen, J.J., Irwin, B., Platt, T., 1983. Autotrophic picoplankton in the tropical ocean. *Science* 219, 292–295.
- Magazzù, G., Decembrini, F., 1995. Primary production, biomass and abundance of phototrophic picoplankton in the Mediterranean Sea: a review. *Aquatic Microbial Ecology* 9, 97–104.
- Martinez-Ruiz, F., Kastner, M., Paytan, A., Ortega-Huertas, M., Bernasconi, S.M., 2000. Geochemical evidence for enhanced productivity during S1 sapropel deposition in the eastern Mediterranean. *Paleoceanography* 15, 200–209.
- Martinez-Ruiz, F., Paytan, A., Kastner, M., Gonzales-Donoso, J.M., Linares, D., Bernasconi, S.M., Jimenez-Espejo, F.J., 2003. A comparative study of the geochemical and mineralogical characteristics of the S1 sapropel in the western and eastern Mediterranean. *Palaeogeography, Palaeoclimatology, Palaeoecology* 190, 23–37.
- Mellor, G.L., Yamada, T., 1982. Development of a turbulence closure model for geophysical fluid problems. *Review of Geophysics and Space Physics* 20, 851–875.
- Mercone, D., Thomson, J., Croudace, I.W., Siani, G., Paterne, M., Troelstra, S., 2000. Duration of S1, the most recent sapropel in the eastern Mediterranean Sea, as indicated by accelerator mass spectrometry radiocarbon and geochemical evidence. *Paleoceanography* 15, 336–347.
- Moutin, T., Rainbault, P., 2002. Primary production, carbon export and nutrient availability in western and eastern Mediterranean Sea in early summer 1996 (MINOS cruise). *Journal of Marine Systems* 33–34, 273–288.
- Murat, A., Got, H., 2000. Organic carbon variations of the eastern Mediterranean Holocene sapropel: a key for understanding formation processes. *Palaeogeography, Palaeoclimatology, Palaeoecology* 158, 241–257.
- Myers, P.G., Haines, K., Rohling, E.J., 1998. Modelling the paleocirculation of the Mediterranean: the last glacial maximum and the Holocene with emphasis on the formation of Sapropel S1. *Paleoceanography* 13, 586–606.
- Olausson E., 1961. Studies of deep-sea cores: *Reports of the Swedish Deep-Sea Expedition, 1947–1948*, 8, 323–438.
- Passier, H.F., Middelburg, J.J., De Lange, G.J., Bottcher, M.E., 1999a. Modes of sapropel formation in the eastern Mediterranean: some constraints based on pyrite properties. *Marine Geology* 153, 199–219.
- Passier, H.F., Bosch, H.J., Nijenhuis, I.A., Lourens, L.J., Bottcher, M.E., Leenders, A., Sinnninghe Damsté, J.S., De Lange, G.J., Leeuw, J.W., 1999b. Sulphic Mediterranean surface waters during Pliocene sapropel formation. *Nature* 397, 146–149.
- Pearce, R.B., Kemp, A.E.S., Koizumi, I., Pike, J., Cramp, A., Rowland, S.J., 1998. A lamina-scale SEM-based study of a late Quaternary diatom-ooze sapropel from the Mediterranean ridge, site 971. In: Robertson, A.H.F., Emeis, K.-C., Richter, C., Camerlenghi, A. (Eds.), *Proc. ODP Sci. Res.*, vol. 160. Ocean Drilling Program, College Station, TX, pp. 349–363.
- Pedersen, T.F., Calvert, S.E., 1990. Anoxia vs. productivity: what controls the formation of organic-carbon-rich sediments and sedimentary rocks? *AAPG Bulletin* 74, 454–466.
- Pinardi, N., Navarra, A., 1993. Baroclinic wind adjustment processes in the Mediterranean Sea. *Deep-Sea Research Part II* 40, 1299–1326.
- Pinardi, N., Zavatarelli, M., Arnieri, E., Crise, A., Ravaoli, M., 2005. The physical, sedimentary and ecological structure and variability of shelf areas in the Mediterranean Sea Chapter 32. Robinson, A.R., Brink, K.H. (Eds.), *The Sea*, vol. 14. Harvard University Press, pp. 1243–1330.
- Rabitti, S., Bianchi, F., Boldrin, A., Ros, L.D., Soccal, G., Totti, C., 1994. Particulate matter and phytoplankton in the Ionian Sea. *Oceanologica Acta* 17, 297–307.
- Redfield, A.C., Ketchum, B.H., Richards, F.A., 1963. The influence of organisms on the composition of seawater. In: Hill, M.N. (Ed.), *The Sea*, vol. 2. Interscience, New York, pp. 26–77.
- Roether, W., Klein, B., Bregant, D., Georgopoulos, D., Beitzel, V., Kovacevich, V., Lucchetta, A., 1996. Recent changes in eastern Mediterranean deep waters. *Science* 271, 333–335.
- Rohling, E.J., 1994. Review and new aspects concerning the formation of eastern Mediterranean sapropels. *Marine Geology* 122, 1–28.
- Rohling, E.J., Gieskes, W.W.C., 1989. Late Quaternary changes in Mediterranean intermediate water density and formation rate. *Paleoceanography* 4, 531–545.
- Rohling, E.J., Jorissen, F.J., De Stigter, H.C., 1997. 200 years interruption of Holocene sapropel formation in the Adriatic Sea. *Journal of Micropaleontology* 16 (2), 97–108.
- Rohling, E.J., Cane, T.R., Cooke, S., Sprovieri, M., Bouloubassi, I., Emeis, K.C., Schiebel, R., Kroon, D., Jorissen, F.J., Lorre, A., Kemp, A.E.S., 2002. African monsoon variability during the previous interglacial maximum. *Earth and Planetary Science Letters* 202, 61–75.

- Rossignol-Strick, M., 1983. African monsoons, an immediate climate response to orbital insolation. *Nature* 304, 46–49.
- Rossignol-Strick, M., 1985. Mediterranean Quaternary sapropels: an immediate response of the African monsoon to variation of insolation. *Palaeogeography, Palaeoclimatology, Palaeoecology* 49, 237–265.
- Ruardij, P., Van Raaphorst, W., 1995. Benthic nutrient regeneration in the ERSEM ecosystem model of the North Sea. *Netherlands Journal of Sea Research* 33 (3/4), 453–483.
- Sachs, J.P., Repeta, D.J., 1999. Oligotrophy and nitrogen fixation during eastern Mediterranean sapropel events. *Science* 286, 2485–2488.
- Slomp, C.P., Thomson, J., De Lange, G.J., 2004. Controls on phosphorus regeneration and burial during formation of eastern Mediterranean sapropels. *Marine Geology* 203, 141–159.
- Smith, C.R., Hoover, D.J., Doan, S.E., Pope, R.H., Demaster, D.J., Dobbs, F.C., Altabet, M.A., 1996. Phytodetritus at the abyssal seafloor across 10° of latitude in the central equatorial Pacific. *Deep-Sea Research II* 43, 1309–1338.
- Stratford, K., Williams, R.G., Myers, P.G., 2000. Impact of the circulation on sapropel formation in the eastern Mediterranean. *Global Biogeochemical Cycles* 14, 685–695.
- Strohle, K., Krom, M.D., 1997. Evidence for the evolution for an oxygen minimum layer at the beginning of S-1 sapropel deposition in the eastern Mediterranean. *Marine Geology* 140, 231–236.
- Van Santvoort, P.J.M., De Lange, G.J., Langereis, C.G., Dekkers, M.J., Paterné, M., 1997. Geochemical and paleomagnetic evidence for the occurrence of “missing” sapropels in eastern Mediterranean sediments. *Paleoceanography* 12, 773–786.
- Varela, R.A., Cruzado, A., Gabaldon, J.E., 1995. Modelling primary production in the North Sea using the European Regional Seas Ecosystem Model. *Netherlands Journal of Sea Research* 33 (3/4), 441–463.
- Vergnaud-Grazzini, C., Ryan, W.B.F., Cita, M.B., 1977. Stable isotope fractionation, climate change and episodic stagnation in the eastern Mediterranean Pleistocene records. *Marine Micropaleontology* 10, 35–69.
- Vichi, M., Oddo, P., Zavatarelli, M., Coluccelli, A., Coppini, G., Celio, M., Fonda Umani, S., Pinardi, N., 2003. Calibration and validation of a one-dimensional complex marine biogeochemical flux model in different areas of the northern Adriatic shelf. *Annales Geophysicae* 21, 413–436.
- Warning, B., Brumsack, H.J., 2000. Trace metal signatures of eastern Mediterranean sapropels. *Palaeogeography, Palaeoclimatology, Palaeoecology* 158, 293–309.
- Wehausen, R., Brumsack, H.J., 1999. Cyclic variations in the chemical composition of eastern Mediterranean Pliocene sediments: a key for understanding sapropel formation. *Marine Geology* 153, 161–176.
- Weldeab, S., Emeis, K.C., Hemleben, C., Schmiedl, G., Schulz, H., 2003. Spatial productivity variations during formation of sapropels s5 and s6 in the Mediterranean Sea: evidence from Ba contents. *Palaeogeography, Palaeoclimatology, Palaeoecology* 191, 169–190.
- Zavatarelli, M., Raicich, M., Bregant, D., Russo, A., Artegiani, A., 1998. Climatological biogeochemical characteristics of the Adriatic Sea. *Journal of Marine Systems* 18, 227–263.